ESD-TR-90-066

(2)

Technical Report
898

AD-A228 218

Materials Systems for 2- to 5-μm Wavelength Diode Lasers

J.N. Walpole
T.C. Harman
S.H. Groves
R.C. Williamson
A.J. Strauss

DTIC
ELECTE
OCT 30 1990
S E D

22 August 1990

Lincoln Laboratory
MASSACHUSETTS INSTITUTE OF TECHNOLOGY
LEXINGTON, MASSACHUSETTS

Prepared for the Department of the Air Force under Contract F19628-90-C-0002.

Approved for public release; distribution is unlimited

This report is based on studies performed at Lincoln Laboratory, a center for research operated by Massachusetts Institute of Technology. The work was sponsored by the Department of the Air Force under Contract F19628-90-C-0002.

This report may be reproduced to satisfy needs of U.S. Government agencies.

The ESD Public Affairs Office has reviewed this report, and it is releasable to the National Technical Information Service, where it will be available to the general public, including foreign nationals.

This technical report has been reviewed and is approved for publication.

FOR THE COMMANDER

Hugh L. Southall

Hugh L. Southall, Lt. Col., USAF
Chief, ESD Lincoln Laboratory Project Office

Non-Lincoln Recipients

PLEASE DO NOT RETURN

Permission is given to destroy this document when it is no longer needed.

MASSACHUSETTS INSTITUTE OF TECHNOLOGY
LINCOLN LABORATORY

MATERIALS SYSTEMS FOR 2- TO 5-μm WAVELENGTH DIODE LASERS

J.N. Walpole
T.C. Harman
S.H. Groves
R.C. Williamson
Group 85

A.J. Strauss
Group 83

Accession For
NTIS GRA&I ☒
DTIC TAB ☐
Unannounced ☐
Justification
By
Distribution/
Availability Codes
Dist | Avail and/or Special
A-1

TECHNICAL REPORT 898

1 NOVEMBER 1988 — 30 SEPTEMBER 1989

ISSUED 22 AUGUST 1990

Approved for public release; distribution is unlimited.

LEXINGTON MASSACHUSETTS

ABSTRACT

Several materials systems are reviewed in an attempt to determine the most favorable for use in the fabrication of diode lasers emitting in the 2- to 5-μm wavelength range. Eight possible systems, along with several of their variations, are identified among the III-V, IV-VI and II-VI semiconductors. All meet the following criteria: optical and carrier confinement can be obtained, a significant portion of the desired wavelength range can be achieved, and the layers that are required to fabricate a double-heterostructure (DH) laser can be lattice matched to a suitable substrate.

The performance of III-V laser devices is limited by Auger recombination and free-carrier absorption. The role of the valence band structure in these effects is of particular importance. The III-V system identified as the most promising is GaInAsSb/AlGaAsSb/GaSb, with the quaternary alloy GaInAsSb for the active layer, the quaternary alloy AlGaAsSb for the cladding layers, and GaSb for the substrate. This system offers substrate availability, a wide range of wavelengths, good metallurgical properties and favorable device physics. In this system, DH lasers emitting at $\approx$ 2.3 μm have been operated CW at room temperature with threshold current densities as low as 1.5 A/cm^2, and differential quantum efficiencies as high as 18 percent per facet have been obtained in pulsed room-temperature operation. According to theoretical projections, the threshold current density of such GaInAsSb/AlGaAsSb/GaSb lasers will increase with increasing wavelength because of increased Auger recombination and free-carrier absorption. In order to reduce these effects and generally improve device performance, we recommend that strained-layer quantum-well devices be investigated.

The IV-VI systems in principle should have less Auger recombination than the III-V systems, as well as less free-carrier absorption, because of the simpler valence band structure of IV-VI materials compared with that of III-V materials. Nevertheless, these effects remain important and limit performance. In addition, the IV-VI systems have much poorer quality of materials and availability of substrates. Among the many undesirable characteristics of the materials are low thermal conductivity and excessive susceptibility to damage during processing. The IV-VI system identified as most favorable is PbEuSSe/PbSe, in which PbEuSSe quaternaries of different alloy compositions are used for both the active and cladding layers, which are lattice matched to PbSe substrates. However, this system is judged less promising than the GaInAsSb/AlGaAsSb/GaSb system.

A possible II-VI laser system is HgCdTe lattice matched to CdZnTe. Yet, this system is not likely to have any advantages over the III-V systems. In addition, it has many disadvantages, including the fact that its materials and device technologies are much less developed.

ACKNOWLEDGMENTS

We are grateful to a number of our colleagues, including Z.L. Liau, S.C. Palmateer, S.J. Eglash, H.J. Zeiger, G.W. Iseler, D.L. Spears, and I. Melngailis, for contributions of research tasks, ideas and discussions helpful to this study. The use of unpublished data of S.J. Eglash and K.A. McIntosh on free-carrier absorption and of S.J. Eglash and H.K. Choi on GaInAsSb/AlGaAsSb diode laser performance is much appreciated. Special thanks are due to K.J. Challberg for editing and greatly improving the manuscript and for expediting preparation of the graphics.

TABLE OF CONTENTS

Abstract		iii
Acknowledgments		v
List of Illustrations		ix
List of Tables		xi
1.	INTRODUCTION	1
1.1	Scope, Major Issues and Criteria of Study	1
1.2	Overview of Materials Systems	4
2.	III-V MATERIALS SYSTEMS	7
2.1	Wavelength vs Lattice Constant	7
2.2	Materials and Growth Issues	7
2.3	Thermal Conductivity	9
2.4	Device Physics	9
2.5	Device Performance	25
2.6	Reliability	30
2.7	Summary	30
3.	IV-VI MATERIALS SYSTEMS	33
3.1	Wavelength vs Lattice Constant	33
3.2	Materials and Growth Issues	34
3.3	Device Physics	35
3.4	Device Performance	40
4.	II-VI MATERIALS SYSTEMS	45
4.1	Wavelength vs Lattice Constant	45
4.2	Materials and Growth Issues	45
4.3	Device Performance	46
5.	BEAM QUALITY	49
6.	SUMMARY AND CONCLUSIONS	53
REFERENCES		55

LIST OF ILLUSTRATIONS

Figure No.		Page
1-1	Basic diode laser structure showing the energy gap variation ΔE_g that provides carrier confinement in the active region.	3
2-1	Wavelength of bandgap radiation vs lattice constant for III-V compounds and alloys. The 2- to 5-μm wavelength region is shaded. The wavelength range available for DH lasers that can be grown lattice matched to binary compound substrates is shown by the three dashed vertical lines.	8
2-2	Two quaternary systems that permit lattice matching to GaSb.	9
2-3	Bandgap of $Ga_xIn_{1-x}As_ySb_{1-y}$ lattice matched to GaSb, with $y = 0.91(1 - x)/(1 + 0.05x)$. Atmospheric transmissions windows that would not be affected by a miscibility gap are shown (diagonal lines).	11
2-4	CHSH and CHCC, two of the most important Auger processes for III-V lasers.	12
2-5	Variation of spin-split-off energy Δ with energy bandgap E_g for many III-V alloys. Adapted from Sugimura [5].	13
2-6	Variation of threshold current density with active layer thickness for $Al_xGa_{1-x}As$/GaAs lasers. Adapted from Casey and Panish [1].	14
2-7	Plots of (a) calculated normalized threshold current densities and (b) calculated radiative efficiencies at threshold for radiative and Auger recombination processes at room temperature in the quaternary III-V alloys GaInPAs/InP, AlGaAsSb/GaSb and GaInAsSb/GaSb. Adapted from Sugimura [5].	15
2-8	Plots of (a) calculated normalized threshold current densities and (b) calculated radiative efficiencies at threshold for radiative and Auger recombination processes at room temperature in the ternary III-V alloys InPAs, InAsSb and GaInSb. Adapted from Sugimura [5].	16
2-9	Plots of (a) calculated normalized threshold current densities and (b) calculated radiative efficiencies at threshold for radiative and Auger recombination processes at 77 K in the ternary III-V alloys InPAs, InAsSb and GaInSb. Adapted from Sugimura [5].	18
2-10	Free-carrier absorption processes.	19
2-11	Intervalley free-carrier absorption in $Ga_{0.63}In_{0.37}Sb$; adapted from Lorenz *et al.* [13]. The dashed curve is recent data for GaSb [14].	20

Figure No.		Page
2-12	Separation of the Γ and L minima, E_0, and the energy bandgap E_g of $Ga_xIn_{1-x}As_ySb_{1-y}$ lattice matched to GaSb, with $y = 0.91(1-x)/(1+0.05x)$.	21
2-13	Intervalence band absorption in GaAs where spin-orbit splitting Δ is 0.34 eV. Adapted from Braunstein and Kane [16].	21
2-14	Intervalence band absorption in AlSb where spin-orbit splitting Δ is 0.075 eV. Adapted from Braunstein and Kane [16].	22
2-15	Qualitative comparison of peak mode gain vs current density in GaAs/AlGaAs laser structures.	23
2-16	Effects of biaxial strain on the valence band structure of III-V semiconductors. Adapted from N.G. Anderson, Ph.D. thesis, North Carolina State University.	24
2-17	Schematic diagram of energy band vs distance for a strained-layer MQW laser. Discrete levels in the wells are not shown. Occupied states under forward-bias conditions are indicated (shaded area).	24
2-18	Predicted threshold current vs temperature for III-V DH lasers. Experiment points are for selected 2.2- to 2.3-μm data, and solid lines represent trends of the data for 0.85-μm GaAlAs and 1.3-μm GaInAsP lasers.	29
3-1	Wavelength vs lattice constant for the PbCdSSe quaternary system.	33
3-2	Wavelength vs lattice constant for PbEuSSe and PbEuTeSe quaternary systems.	34
3-3	Variation of (a) energy gap with alloy composition and (b) electron mobility with alloy composition for some lead salt alloys. Adapted from Partin [44].	36
3-4	Estimated variation of energy gap in the PbEuSe ternary system.	37
3-5	PbS energy band structure near the energy gap along the **k** axis from Γ to L. Position along the **k** axis is denoted by the group theoretical symbols Γ, Λ and L.	38
3-6	Experimental free-carrier absorption in PbS at 300 K.	39
3-7	Maximum operating temperature vs wavelength for III-V and IV-VI lasers. The solid lines and the dashed line are discussed in the text. Adapted from Horikoshi [55].	42

Figure No.		Page
3-8	Experimental threshold currents vs temperature for some IV-VI lasers compared with III-V predictions.	42
4-1	Wavelength vs lattice constant for the HgCdZnTe quaternary system.	45

LIST OF TABLES

Table No.		Page
1-1	Effect of Materials and Device Physics Issues on System Requirements for Diode Lasers	2
1-2	Potential Alloy Systems for 2- to 5-μm Diode Lasers	4
2-1	Thermal Properties of Compounds and Alloys	10
2-2	Device Summary for Diode Lasers with GaInAsSb Active Layer Emitting at 2.2 to 2.3 μm.	26
2-3	Device Summary for 2- to 4-μm Diode Lasers Using III-V Compounds with Active Regions Other Than GaInAsSb	27
3-1	Device Summary for 3- to 5-μm Diode Lasers Using IV-VI Compounds	41
4-1	Device Summary for Diode Lasers Using II-VI Compounds	46

1. INTRODUCTION

1.1 SCOPE, MAJOR ISSUES AND CRITERIA OF STUDY

The major issues raised by the system requirements for high-power semiconductor diode lasers emitting in the 2- to 5-μm wavelength range are (1) wavelength coverage obtainable, (2) producibility, (3) efficiency and maximum power limitations, (4) reliability, (5) tunability and (6) beam quality. The first three of these issues will be the main emphasis of this study, since they are related to numerous details of the materials properties and device physics. These are issues about which information can be obtained and choices and decisions can be made.

The remaining three issues are less suitable for study. Reliability cannot be predicted with confidence from available data or theory. A brief discussion of general trends and known problems is included as we review specific semiconductor materials systems. Tunability is not addressed further since it is easily dealt with now. Variation of operating temperatures is the most practical scheme with a tuning rate of about 3×10^{-4} eV/K. Assuming $\pm$ 10 K is possible, one could, for example, operate lasers at 2.25 ± 0.013, 3.75 ± 0.034 or 4.75 ± 0.055 μm. More than twice these tuning ranges could be achieved using external cavity techniques, but that approach would significantly increase system complexity. Much wider tunability is probably not practical. Finally, obtaining good beam quality from diode lasers operating in the 1- to 10-W range is a matter of much current interest with considerable research and development under way. Various approaches for achieving diffraction-limited, high-power beams are described and discussed briefly in Section 5. However, the issue is a general one and does not influence the choice of the most promising materials system for long-wavelength lasers.

From a materials perspective, the problem reduces to growth of appropriate heterostructures with sufficient crystalline quality while maintaining adequate control of all the growth parameters. The materials issues have the major impact on the questions of producibility and wavelength coverage, the latter being totally determined by the materials system or systems chosen, as shown in Table 1-1. Considerations of device physics, on the other hand, mainly determine the limitations on efficiency and maximum power. These are ultimately related to the laser threshold current and the quantum efficiency, which are determined by several factors as listed in Table 1-1.

Auger recombination and free-carrier absorption significantly influence performance limitations for all long-wavelength lasers. Auger recombination is a nonradiative process in which the energy of the recombining electron-hole pair is used to increase the energy of a third free carrier rather than to produce light. This process robs carriers and hence available gain from the stimulated emission process and greatly increases the threshold current. Free-carrier absorption causes internal optical loss and therefore not only increases threshold current but also reduces external quantum efficiency. As will be shown, two of the most troublesome free-carrier absorption processes for III-V materials systems involve intervalence band absorption between the spin-split-off band and the heavy-hole band at short wavelengths in the 2- to 5-μm range and between the

light-hole band and the heavy-hole band at long wavelengths in the same range. At short wavelengths, an intervalley absorption process in the conduction band is also an issue. Free-carrier absorption and Auger recombination should be less important in the lead salt materials systems, but they remain limiting factors. Also, in the lead salt systems the electrical conductivity, thermal conductivity and carrier confinement may provide other limitations.

We assume that carrier and optical confinement must be obtainable using a basic lattice-matched, double-heterostructure (DH) laser for any candidate materials system. More sophisticated structures may also be desirable as discussed later. Figure 1-1 depicts a basic DH structure and shows the energy gap variation with distance that provides carrier confinement in the active region. It is assumed, of course, that a *p-n* junction is in or quite near the active region. Carrier confinement depends on ΔE_C and ΔE_V, the discontinuities in the conduction band and the valence

TABLE 1-1

Effect of Materials and Device Physics Issues on System Requirements for Diode Lasers

Issue	System Requirement			
	Wavelength Coverage	Efficiency	Maximum Power	Producibility
Materials				
Materials system	x			x
Substrate quality				x
Epitaxial growth				x
Device physics				
Auger recombination		x	x	
Free-carrier absorption		x	x	
Electrical conductivity		x	x	
Thermal conductivity			x	
Optical and carrier confinement		x	x	

x = Issue has a significant effect on the system requirement.

band, respectively, rather than simply on the energy gap variation ΔE_g ($\Delta E_g = \Delta E_C + \Delta E_V$). Moreover, lack of confinement, or leakage of carriers out of the active layer, involves not only ΔE_C and ΔE_V but also detailed solutions of Poisson's equation, the populations of carriers in higher energy bands, the optical confinement factor, and carrier transport effects [1]. In GaAs/ $Ga_{1-x}Al_xAs$ layers, leakage is not minimized until $x \geq 0.3$, where $\Delta E_g \geq 0.37$ eV. For room-temperature operation, we will assume that an energy gap difference at least on the order of 0.4 eV will be required.

The confinement layers in Figure 1-1 are also termed *cladding* layers because of their role in forming the cladding regions of an optical waveguide. In general, the active layer has an optical index n_a which is greater than the optical index n_c of the cladding layers. The optical confinement factor Γ is the fraction of the energy of the optical mode confined to the active layer of thickness d. From standard guided-wave theory one can calculate that if

$$\frac{\pi d\sqrt{n_a^2 - n_c^2}}{\lambda} \geq 0.5 \tag{1.1}$$

then $\Gamma \geq 0.39$. Here, λ is the optical wavelength. For comparison purposes, we will take $\Gamma \geq 0.39$ as a standard requirement for conventional DH lasers.

In more advanced structures having separate optical and carrier confinement, there are layers of intermediate composition located between the cladding and the active layers. Careful control and optimization of the composition, thickness and doping of these intermediate layers are important to ultimate performance.

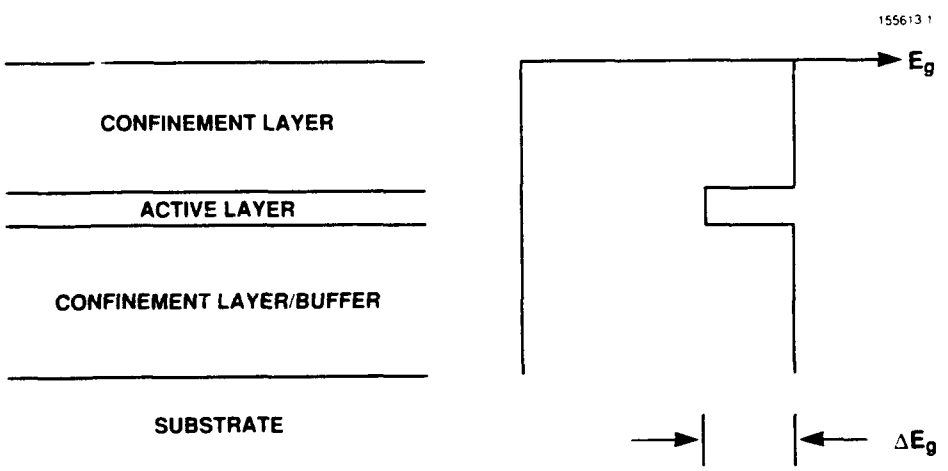

Figure 1-1. Basic diode laser structure showing the energy gap variation ΔE_g that provides carrier confinement in the active region.

1.2 OVERVIEW OF MATERIALS SYSTEMS

With optical and carrier confinement, wavelength coverage and lattice matching as criteria, potential materials systems for basic DH lasers in the 2- to 5-μm wavelength region have been identified. These are grouped by compounds and alloys as III-V, IV-VI and II-VI systems, even though other elements (often column II) are frequently substituted for the IV element in IV-VI materials systems. The alloys used for the active layer, confinement layers and substrate for each of the possible systems are listed in Table 1-2, which also notes those systems that are shown by this study to have the most promise based on their materials and device physics properties.

The GaInAsSb/AlGaAsSb system was identified early in the study as the most promising of the III-V systems. However, published theoretical calculations suggested that Auger recombination might be an extremely serious obstacle to achieving good room-temperature performance of lasers in this system, although there were some experimental data suggesting that this was not the case.

TABLE 1-2

Potential Alloy Systems for 2- to 5-μm Diode Lasers

Materials System	Active Layer	Confinement Layers	Substrate
III-V	GaInAsSb*	AlGaAsSb*	GaSb,* InAs
	AlInAsSb	AlInAsSb	GaSb, InAs
	InPAsSb	InPAsSb	GaSb, InAs
	GaInAsSb	GaAlInSb	GaInSb
IV-VI†	PbEuSSe*	PbEuSSe*	PbSe*[$BaSrF_2$]
	PbEuSeTe	PbEuSeTe	PbTe
	PbCdSSe	PbCdSSe	PbS
II-VI	HgCdTe	HgCdTe	CdZnTe

* Systems that show the most promise for this application.
† Sr, Ca, Ba, Zn and others are possible in place of Eu in the IV-VI quaternaries.

Since then, the performance of lasers fabricated at Lincoln Laboratory from GaInAsSb/AlGaAsSb structures grown by molecular beam epitaxy (MBE) has confirmed that Auger recombination is substantially less probable than calculated theoretically, considerably improving the prospects for the development of high-performance lasers in this materials system.

The quaternary alloy system GaInAsP/InP is not included in Table 1-2. This system could in principle be used in the wavelength range close to 2 μm if strained-layer quantum-well lasers can be successfully made. However, its wavelength range is very limited and its Auger recombination rate is likely to be large. GaInAsP/InP has no known advantages over the other systems except its more developed technology, and it is not considered in detail here. As discussed in Section 2.4.3, if strained-layer quantum-well lasers in GaInAsSb/AlGaAsSb/GaSb are not successful it may be productive to look again at this more familiar system.

The III-V, IV-VI and II-VI materials systems are discussed separately in Sections 2, 3 and 4, which review materials and device physics issues in relation to wavelength coverage, summarize device results to date and where appropriate make projections for ultimate performance. Section 5 is a brief discussion of beam quality, and Section 6 provides conclusions and recommendations.

2. III-V MATERIALS SYSTEMS

2.1 WAVELENGTH VS LATTICE CONSTANT

The wavelength of optical radiation and the energy gap vs the lattice constant for several III-V compounds are plotted in Figure 2-1. GaP and AlP are omitted for simplicity. Lines connecting the compounds represent ternary alloys. For example, the wavelength vs lattice constant for $Ga_{1-x}In_xSb$ is given by the line connecting GaSb to InSb with x increasing from 0 to 1 along that line. Any point inside the lines can be reached by some quaternary alloy. For example, $Ga_{1-x}In_xAs_{1-y}Sb_y$ can be obtained inside the region bounded by GaAs, InAs, InSb and GaSb and by the ternary lines connecting these compounds. The diagram is drawn using the energy gaps at 77 K and would look slightly different at room temperature where these values would shrink by about 70 meV.

Among possible substrates, AlSb permits the largest range of wavelength for lattice-matched active layers, but it is not available in bulk form. InAs provides the poorest wavelength range. GaSb appears most promising since it has a range that extends to about 4.3 μm at room temperature and is available in bulk form. An additional feature of GaSb which may be of use in advanced surface-emitting structures is that the substrate is transparent and light can be extracted through it.

There are three possible quaternary alloys that can be used for the active layer, all of which contain In and Sb since InSb must be an endpoint for any alloy at long wavelength. The three systems are InPAsSb, InAlAsSb and InGaAsSb. Metallurgically, the latter is preferable. It is better than InAlAsSb since it substitutes Ga for Al, a troublesome alloy constituent because it is so highly reactive. InPAsSb is a poor system metallurgically because it contains three different group V elements with different atomic radii.

For the cladding layers there are four possible quaternary systems, all of which contain Sb and Al. Sb is necessary and Al desirable in order to obtain large carrier and optical confinement. AlGaAsSb has the best metallurgical properties compared with the other three, AlInPSb, AlGaPSb and AlInAsSb. This superiority results from the similarity of atomic radii; Al and Ga have very similar radii, and As and Sb are much closer than P and Sb.

Figure 2-2 is a simplified diagram of wavelength vs lattice constant for only the compounds and bounding ternaries relevant to the two quaternary systems selected, GaInAsSb for the active layer and AlGaAsSb for the cladding layers, both lattice matched to GaSb substrates.

2.2 MATERIALS AND GROWTH ISSUES

Even when materials systems with the best metallurgical properties are used there may be problems. Two difficulties have been noted in liquid-phase epitaxial (LPE) growth of the quaternaries mentioned above. The first is the problem of achieving lattice matching when growing

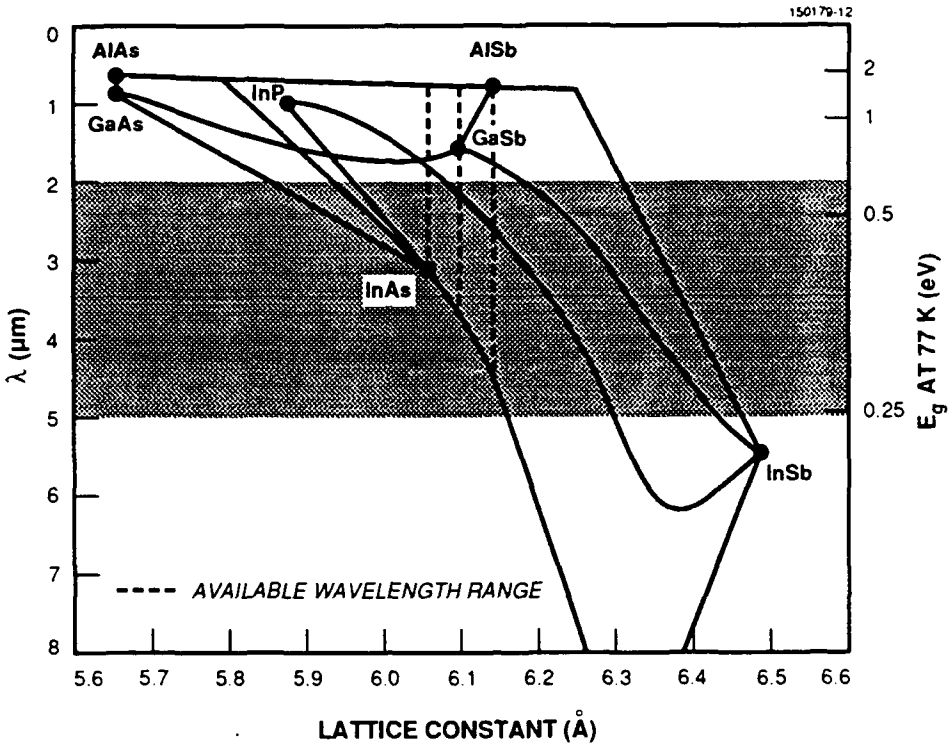

Figure 2-1. Wavelength of bandgap radiation vs lattice constant for III-V compounds and alloys. The 2- to 5-μm wavelength region is shaded. The wavelength range available for DH lasers that can be grown lattice matched to binary compound substrates is shown by the three dashed vertical lines.

AlGaAsSb on GaSb because of the limited solubility of As in the melt [2]. This difficulty could be solved by using, for example, MBE growth where no such solubility limitation occurs. The second problem is the potential for a miscibility gap in the GaInAsSb system. According to one report [3], in order to obtain a certain compositional range in an equilibrium growth process the temperature must be increased above the melting point of the GaSb substrate. Hence, that range would be inaccessible. This miscibility gap is not well documented and has not been reported with MBE growth, where equilibrium arguments may not apply. Growth by MBE of GaInAsSb lattice matched to GaSb with a mole fraction of In up to 0.26 has been described [4]. Comparing this report with the theory of Reference 3, we conclude that the maximum effect of the miscibility gap (if any) for MBE growth would be to preclude devices operating in a portion of the wavelength range. Figure 2-3 shows the wavelength vs composition at 77 and 300 K with the possible gap region indicated by the dashed portions of the curves. The atmospheric transmission windows indicated by the diagonal lines would not be affected by such a gap.

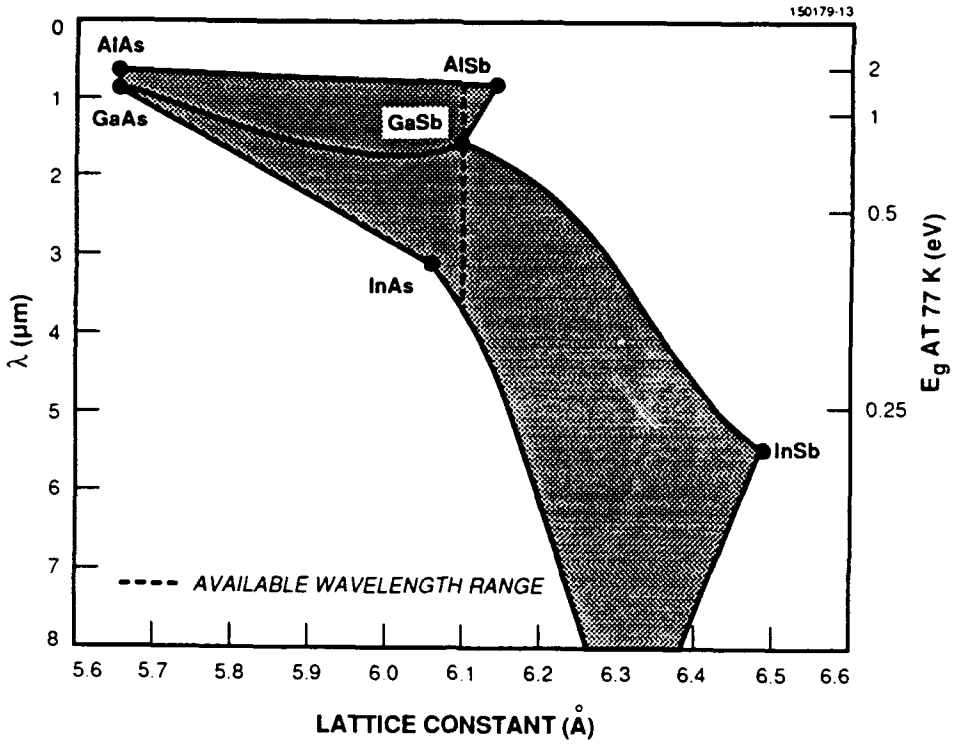

Figure 2-2. Two quaternary systems that permit lattice matching to GaSb.

2.3 THERMAL CONDUCTIVITY

A separate materials consideration is thermal conductivity, especially in alloys where scattering may severely decrease this parameter. Table 2-1 is a compendium of experimental and theoretical values of thermal conductivity as well as the thermal coefficients of expansion for a number of III-V, IV-VI and II-VI materials. (As reference points, the thermal conductivity of copper is 400 W/mK and of silicon is 145 W/mK.) It should be noted that the III-V materials generally have better thermal conductivity than other materials even when III-V alloys are compared, for example, with the IV-VI binary compounds. Nevertheless, alloy scattering leads to lower values of thermal conductivity. Fortunately, layer thicknesses are small (a few micrometers), and the AlGaAsSb cladding layers should be similar to the AlGaAs confinement layers used in GaAs lasers. In fact, if $AlAs_{0.08}Sb_{0.92}$ is used the calculated value is 28, which is quite good.

2.4 DEVICE PHYSICS

In order to interpret the performance reported in long-wavelength III-V lasers and to predict ultimate performance, we need to consider issues of device physics. As mentioned earlier, Auger

TABLE 2-1

Thermal Properties of Compounds and Alloys

Materials System	Compound	Conductivity at 300 K (W/mK)	Coefficient of Expansion ($\times 10^6 K^{-1}$)
III-V	AlAs	91.0	5.2
	$AlAs_{0.08}Sb_{0.92}$	28.0	-
	$Al_{0.5}Ga_{0.5}As$	11.7	-
	AlSb	57.0	-
	GaAs	44.0	6.4
	$Ga_{0.5}In_{0.5}As$	4.8	-
	$Ga_{0.5}In_{0.5}Sb$	4.3	-
	$Ga_{0.8}In_{0.2}As_{0.175}Sb_{0.825}$	5.4	-
	GaSb	40.0	6.1
	InAs	27.0	4.7
	$InP_{0.5}As_{0.5}$	8.9	-
	InP	68.0	4.6
IV-VI	PbS	3.0	20.0
	PbSe	1.7	19.0
	PbTe	2.0	20.0
II-VI	CdTe	7.0	5.3
	$Hg_{0.5}Cd_{0.5}Te$	2.0	-
	HgTe	2.0	5.1
	ZnTe	16.0	8.8
Fluorides	BaF_2	10.0	20.0
	SrF_2	-	19.0

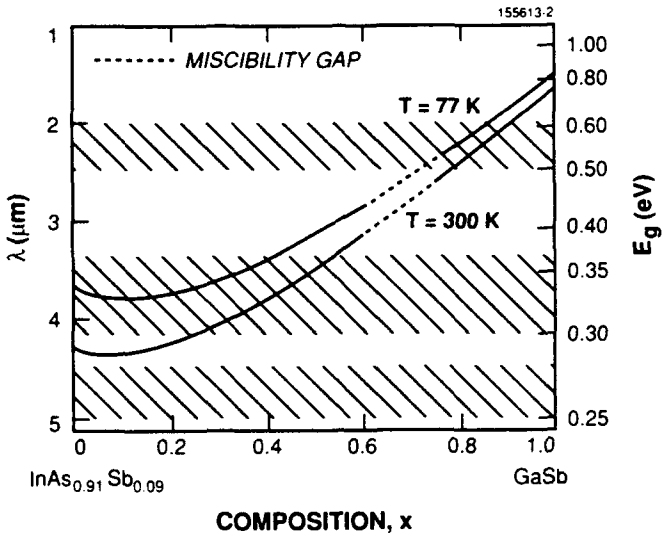

Figure 2-3. Bandgap of $Ga_xIn_{1-x}As_ySb_{1-y}$ lattice matched to GaSb, with $y = 0.91(1 - x)/(1 + 0.05x)$. Atmospheric transmissions windows that would not be affected by a miscibility gap are shown (diagonal lines).

recombination and free-carrier absorption are the major problems limiting device performance. In this section we discuss these difficulties and how they may be decreased by the use of structures more advanced than the basic DH laser.

2.4.1 Auger Recombination

The extensive list of theoretical literature on Auger recombination includes many recent treatments of this process in the 1.3- and 1.5-μm quaternaries lattice matched to InP. Sugimura [5] has made calculations for many III-V alloys including those of interest here, and his calculations will be presented and used for estimating threshold current densities of DH lasers.

Two of the most important Auger processes are illustrated in Figure 2-4. The first is CHSH, involving electrons located in the conduction, heavy-hole, spin-split-off and heavy-hole bands. An electron in the conduction band goes to the heavy-hole band (recombines with a hole), while an electron in the spin-split-off band goes to the heavy-hole band. Energy and momentum are conserved in the process. CHSH is distinguished by the movement of an electron from the spin-split-off band. The second process illustrated in Figure 2-4 is CHCC, which is distinguished by the excitation of an electron that remains in the conduction band; this is the classic Auger process originally calculated by Beattie and Landsberg [6]. Another process that may be significant is

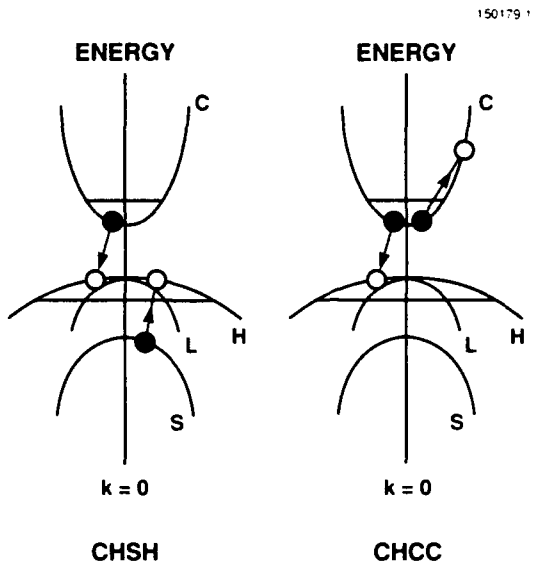

Figure 2-4. CHSH and CHCC, two of the most important Auger processes for III-V lasers.

CHLH, which is characterized by the movement of an electron from the light-hole band to the heavy-hole band.

The Auger rate r_C of the CHCC process is proportional to a statistical factor which, neglecting nonparabolicity of the energy bands, is approximately

$$r_C \propto \exp\left(-\frac{\mu E_g}{kT}\right), \tag{2.1}$$

where μ is the ratio of conduction band mass m_C to heavy-hole band mass m_H, E_g is the energy gap, k is Boltzmann's constant and T is the temperature in kelvins. Small values of μ and E_g both lead to large Auger rates. The energy Δ of the splitting between the heavy-hole and spin-split-off bands plays an important role in the Auger rate r_S of the CHSH process. For $E_g < \Delta$

$$r_S \propto \exp\left[-\frac{(\Delta - E_g)}{kT}\right], \tag{2.2}$$

and for $E_g > \Delta$

$$r_S \propto \exp\left[-\frac{\mu'(E_g - \Delta)}{2kT}\right], \tag{2.3}$$

where μ' is the ratio of the spin-split-off to heavy-hole band masses. Here, it is apparent that $\Delta \approx E_g$ is undesirable and that for a given magnitude of $\Delta - E_g$ the condition $\Delta > E_g$ is better than $\Delta < E_g$, since generally $\mu' < 1$ and there is an extra factor of 2 in the denominator of the exponent in Equation (2.3).

The relationship between the spin-split-off gap Δ and the energy gap E_g is also important in the discussion of the intervalence band absorption that dominates the p-type free-carrier absorption discussed in Section 2.4.2. Figure 2-5 is adapted from Sugimura's work [5], with some errors corrected, and shows the relationship between Δ and E_g for the alloys of interest. The range of band gaps corresponding to the 2- to 5-μm wavelength range is $0.25 \leq E_g \leq 0.6$ eV. It is clear that the condition $\Delta > E_g$ is satisfied by the GaInAsSb/GaSb and AlGaAsSb/GaSb systems.

Sugimura also calculated the normalized threshold current density given by J_{th}/d, where J_{th} is the threshold current density (in kA/cm^2) and d is the active layer thickness (in μm). The meaning of the normalized current density is better understood by looking at the curves for $Al_xGa_{1-x}As$/GaAs lasers in Figure 2-6. Here, we see that the normalized threshold current density is the slope of the line representing J_{th} vs d in the limit of large d and has a value of about 5 kA/cm^2 μm for GaAs. It is possible to reduce the threshold by reducing d. The limit to how small the threshold can

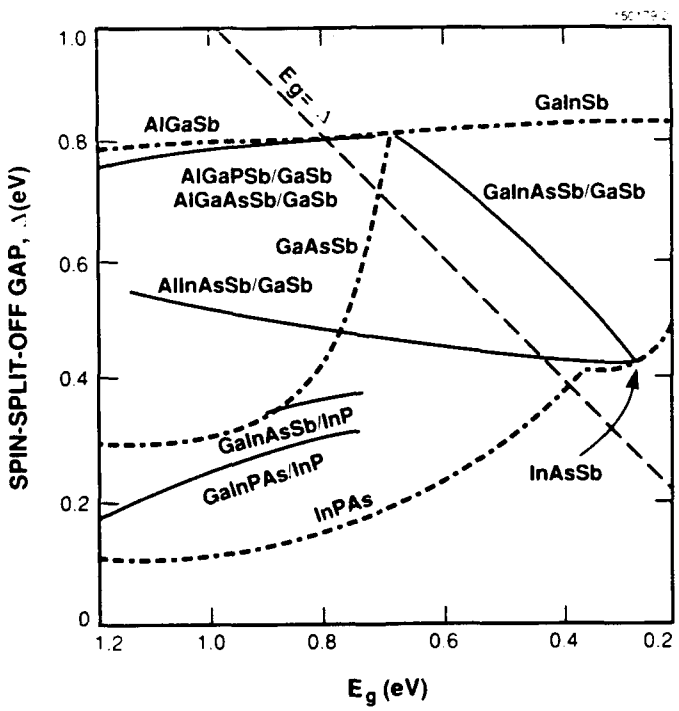

Figure 2-5. Variation of spin-split-off energy Δ with energy bandgap E_g for many III-V alloys. Adapted from Sugimura [5].

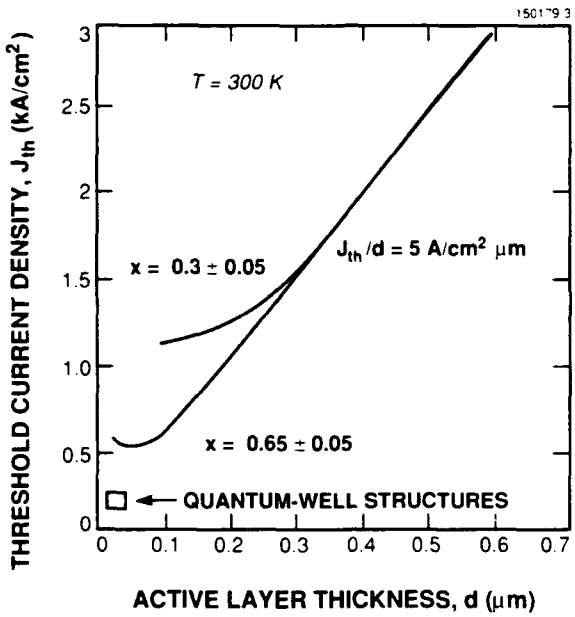

Figure 2-6. Variation of threshold current density with active layer thickness for $Al_xGa_{1-x}As/GaAs$ lasers. Adapted from Casey and Panish [1].

be depends upon the structure and hence the optical confinement. With quantum-well structures in GaAs, threshold current densities have been obtained as small as about 0.1 kA/cm^2.

Since laser performance using the quaternary GaInPAs lattice matched to InP is familiar, we show Sugimura's results for this materials system in Figure 2-7. Also illustrated are calculations for the alloy of most interest, GaInAsSb/GaSb, and for the alloy that would be the cladding layer for the laser system, AlGaAsSb/GaSb. In each calculation the various components of the total current are shown as $J_{th} = J_S + J_C + J_L + J_{rad}$, where the J_S, J_C and J_L denote the current required by the Auger processes CHSH, CHCC and CHLH, respectively, and J_{rad} is the current contributing to radiative recombination. J_{rad}/J_{th} is the radiative efficiency at threshold, which is also shown in Figure 2-7 for each of the three alloys. It should be emphasized that this efficiency is not the differential quantum efficiency above threshold that is most frequently measured in lasers. For example, for the quaternary lattice matched to InP at 1.3 μm the radiative efficiency is only about 35 percent, but differential quantum efficiency above threshold has been reported [7] approaching 70 percent.

Figure 2-8 shows the calculated normalized threshold current density and radiative efficiencies for three ternaries with energy gaps in the region of interest. Both GaInSb and InAsSb are very similar to GaInAsSb/GaSb. For all three the dependence of J_{rad} and J_C on bandgap is

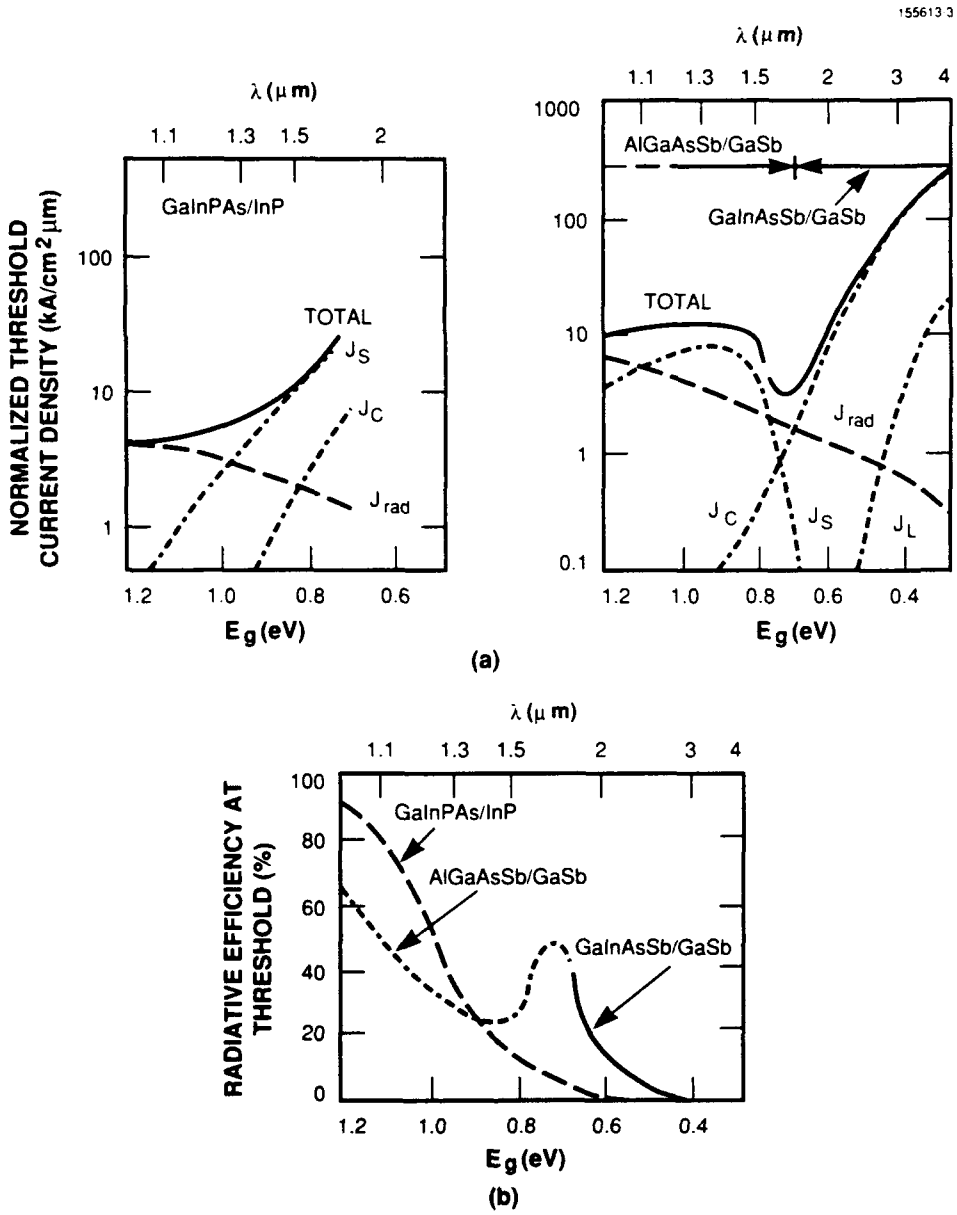

Figure 2-7. Plots of (a) calculated normalized threshold current densities and (b) calculated radiative efficiencies at threshold for radiative and Auger recombination processes at room temperature in the quaternary III-V alloys GaInPAs/InP, AlGaAsSb/GaSb and GaInAsSb/GaSb. Adapted from Sugimura [5].

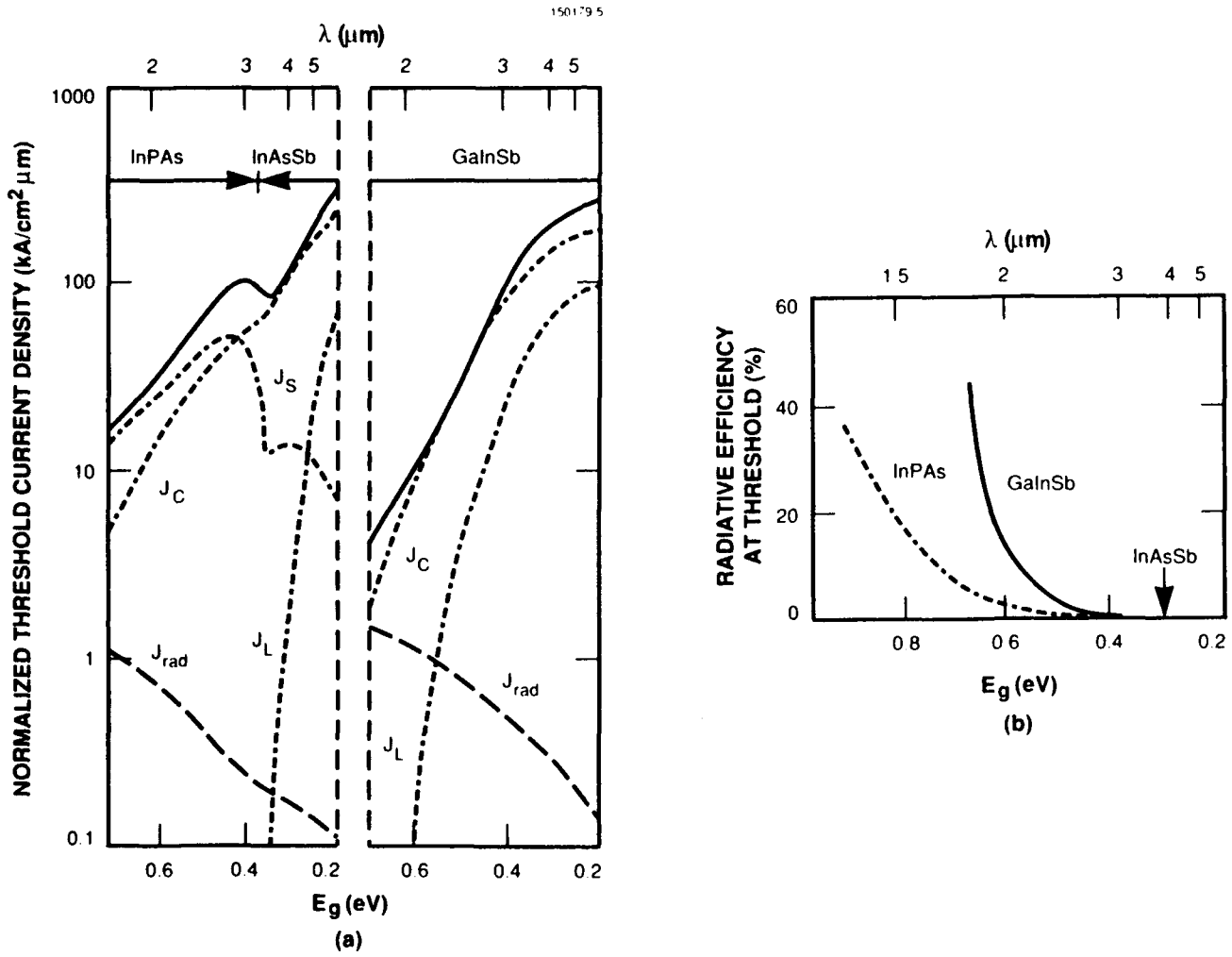

Figure 2-8. Plots of (a) calculated normalized threshold current densities and (b) calculated radiative efficiencies at threshold for radiative and Auger recombination processes at room temperature in the ternary III-V alloys InPAs, InAsSb and GaInSb. Adapted from Sugimura [5].

similar, and J_S is relatively unimportant since $\Delta > E_g$. GaInSb is most like the quaternary GaInAsSb; for example, it shows a similar dependence of J_L on bandgap. For this reason we can use Sugimura's calculations of threshold for GaInSb at 77 K to get an idea of the temperature dependence expected in the quaternary. (No low-temperature calculations for the quaternary were reported.) These calculated results for GaInSb along with the other ternaries in Figure 2-8 are shown in Figure 2-9. Note that out to about 3.5-μm wavelength the radiative current dominates. This component is relatively independent of alloy system at room temperature and varies relatively slowly with temperature compared with the Auger components. The only significant difference between GaInSb and InAsSb is the larger J_L component in GaInSb. This component is not very important in any case at 77 K. Both GaInAsSb/GaSb and GaInSb should be essentially dominated by J_{rad} and J_C and hence almost entirely determined by the conduction and heavy-hole bands, which are very similar for the two systems.

2.4.2 Free-Carrier Absorption

Four kinds of free-carrier absorption in the III-V alloys are illustrated in Figure 2-10. The α_{CC} process in the conduction band is the simplest type. It generally is linearly proportional to the carrier density and for most semiconductors increases with wavelength as λ^p, where p is between 2 and 3.5. According to available data [8], if carrier densities in the confinement regions are around 10^{18} cm^{-3} or less this absorption should be less than 10 cm^{-1}. For densities of 2×10^{18} cm^{-3} in the active layer this process would contribute less than 20 cm^{-1}.

Another absorption process is α_{Csm}, the transition of conduction band electrons from the zone-centered minimum at Γ to a secondary minimum sm of the conduction band, which usually occurs at L. Such intervalley free-carrier absorption has been observed in a number of III-V compounds and alloys, including GaAs [9],[10], InP [11], GaSb [12] and GaInSb [13]. The latter study is of particular interest since relevant values of the absorption coefficient were given, and a figure from it is modified in Figure 2-11. The exact concentration of electrons was not given, but judging from the information provided we estimate it to be approximately 8 to 9×10^{17} cm^{-3}. The energy gap of this alloy is about 0.55 eV, corresponding to $\lambda = 2.25$ μm, where the intervalley absorption α_{Csm} is on the order of 50 cm^{-1}. If at laser threshold the injected carrier density is on the order of 2×10^{18} cm^{-3}, then we extrapolate that α_{Csm} will contribute approximately 120 cm^{-1} of loss in the active layer. (All free-carrier absorption processes are essentially linearly dependent on free-carrier concentration.)

A measurement [14] of the absorption coefficient in n-type GaSb was done recently at Lincoln Laboratory as part of a program to develop GaInAsSb/AlGaAsSb/GaSb lasers. These results are included in Figure 2-11. Here the absorption coefficient is about 9 cm^{-1} for a concentration of 5×10^{17} cm^{-3}. For 2×10^{18} cm^{-3}, we extrapolate $\alpha_{Csm} \approx 36$ cm^{-1}. This value is much smaller than the value extrapolated for that concentration from the data of Reference 13 for GaInSb, even though the energy of the Γ and L splitting, E_0, is much less (about 0.08 eV in GaSb

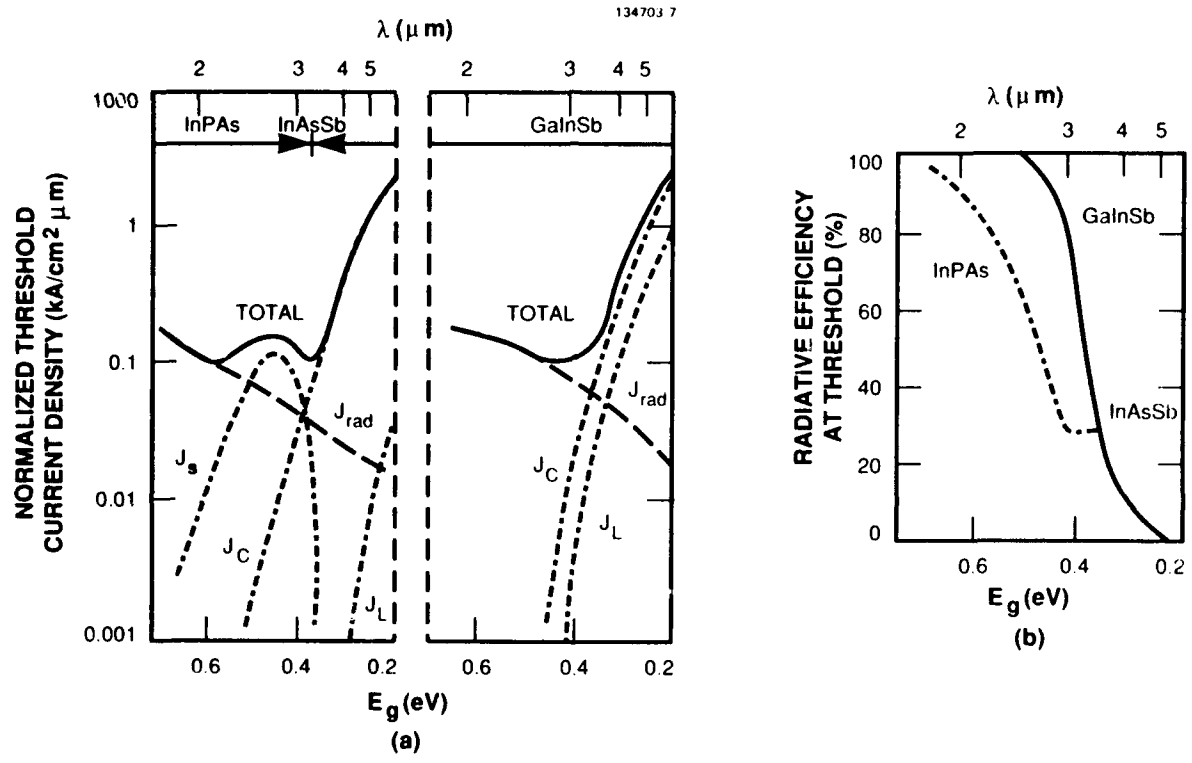

Figure 2-9. Plots of (a) calculated normalized threshold current densities and (b) calculated radiative efficiencies at threshold for radiative and Auger recombination processes at 77 K in the ternary III-V alloys InPAs, InAsSb and GaInSb. Adapted from Sugimura [5].

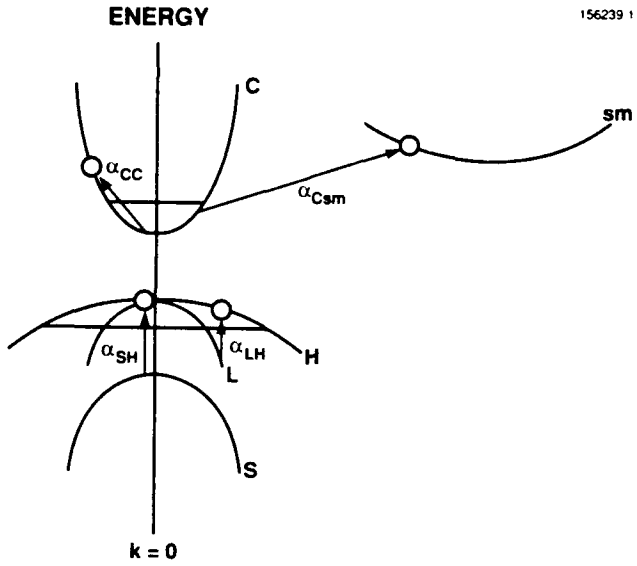

Figure 2-10. Free-carrier absorption processes.

vs about 0.23 eV in the GaInSb alloy). The reason for such a large difference in the absorption coefficient in the two cases is not clear. Further work is needed to predict the absorption for the GaInAsSb/AlGaAsSb/GaSb lasers.

Figure 2-12 shows E_0 in GaInAsSb lattice matched to GaSb along with E_g at 300 K. The values for E_0 are estimated by linear extrapolation from data [15] for the binary compounds InAs, InSb and GaSb. Near pure GaSb the value of E_0 is not shown, but as stated above it reaches about 0.08 eV. For an energy gap similar to the value of 0.55 eV in Reference 13, the value of E_0 is also similar to the value in Reference 13. Hence, in the worst case one might expect that intervalley absorption coefficients will be similar in this wavelength range. The use of InAs rather than GaSb as the substrate might reduce this absorption. For wavelengths longer than 3 μm, $E_0 > E_g$, and this process will no longer be important. Unfortunately, in the AlGaAsSb cladding the separation between the lowest and secondary minima of the conduction band [15] remains < 0.3 eV for any composition. It may be important to keep carrier densities low in the *n*-type cladding layer near the active layer where the optical mode has appreciable amplitude.

Intraband absorption similar to the α_{CC} process can occur in the valence band of the active layer and the *p*-type cladding region. However, in general it is far outweighed by interband absorption effects. The two most important are α_{SH}, the absorption of light by an electron in the spin-split-off band which makes a transition to an empty level in the heavy-hole band, and α_{LH}, the absorption of light by an electron in the light-hole band which makes a transition to the heavy-hole band. These effects are shown in Figure 2-10. A process similar to α_{SH} but with the final state in the light-hole band, α_{SL}, also occurs. However, this is comparatively unimportant since

there are relatively few light holes and the matrix element is between states of nominally the same parity and therefore small. The α_{LH} transitions are low energy compared with the α_{SH} transitions, so we may think of them as contributing to absorption at long and short wavelengths, respectively. In fact, if spin-orbit splitting Δ for the active and p-type confinement regions is large enough compared with the energy gap of the active region, the α_{SH} transitions may not be a problem in the 2- to 5-μm range. As illustrated in Figure 2-5, the value of Δ for the p-type confinement region is near 0.8 eV for AlGaAsSb/GaSb and approximates E_g + 0.13 eV for GaInAsSb/GaSb active layers.

The absorption coefficient vs photon energy is plotted in Figure 2-13 for p-type GaAs ($p = 2.7 \times 10^{17}$ cm^{-3}) at room temperature [16] where Δ = 0.34 eV. Intervalence band absorption has been observed in InP [17], GaSb [12], GaP [18], GaInAsP [19], InAs [20] and AlSb [16]. The GaSb data are not detailed enough to be useful, but the AlSb results are of interest since the cladding material may be very similar. Figure 2-14 shows the intervalence band

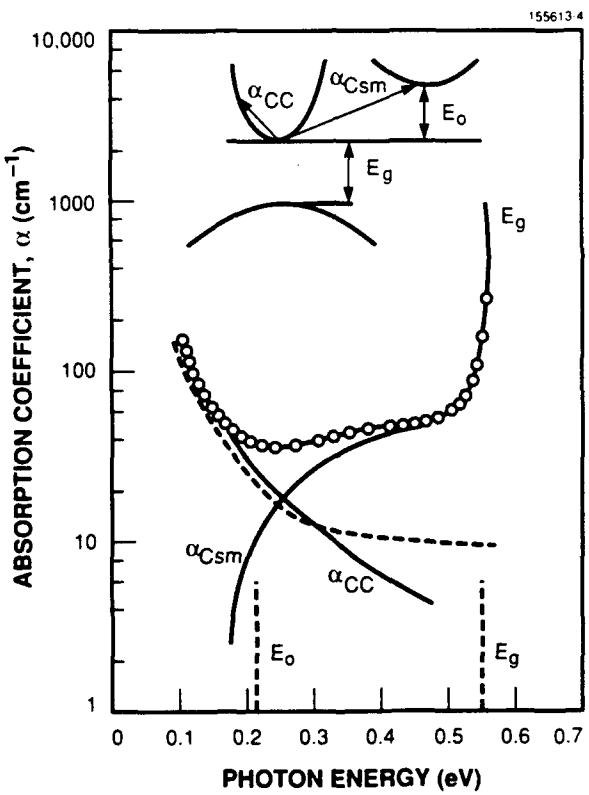

Figure 2-11. Intervalley free-carrier absorption in $Ga_{0.63}In_{0.37}Sb$; adapted from Lorenz et al. [13]. The dashed curve is recent data for GaSb [14].

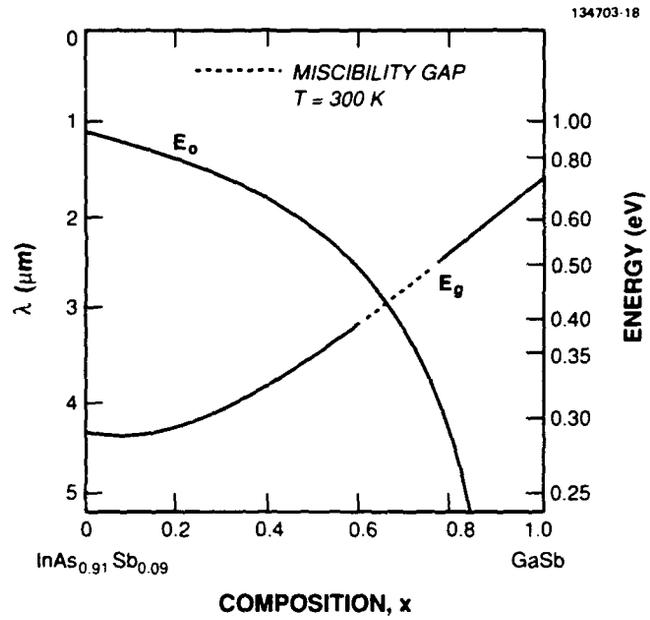

Figure 2-12. Separation of the Γ and L minima, E_0, and the energy bandgap E_g of $Ga_xIn_{1-x}As_ySb_{1-y}$ lattice matched to GaSb, with $y = 0.91(1 - x)/(1 + 0.05x)$.

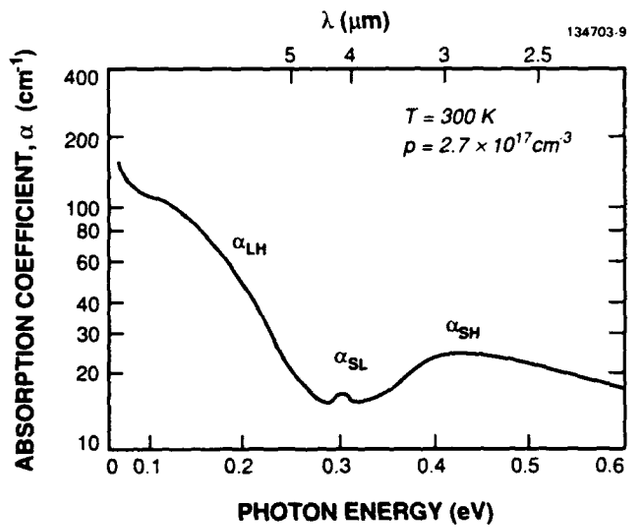

Figure 2-13. Intervalence band absorption in GaAs where spin-orbit splitting Δ is 0.34 eV. Adapted from Braunstein and Kane [16].

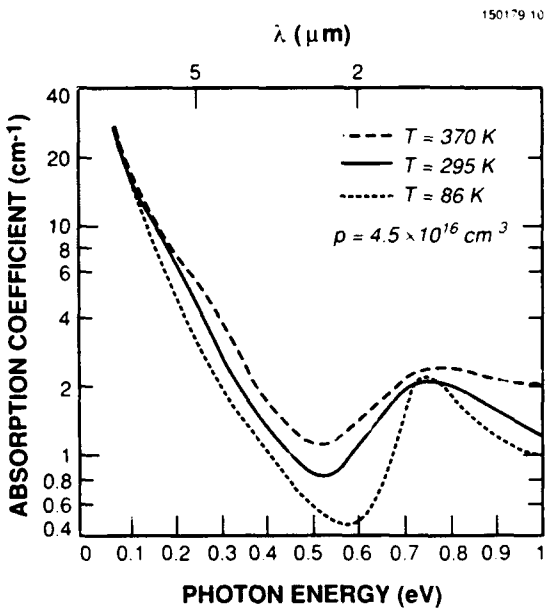

Figure 2-14. Intervalence band absorption in AlSb where spin-orbit splitting Δ is 0.075 eV. Adapted from Braunstein and Kane [16].

absorption for 4.5×10^{16} cm^{-3} AlSb where $\Delta = 0.75$ eV. At room temperature the values of α vary from less than 1 cm^{-1} for short wavelengths (0.4 to 0.6 eV) up to about 5 cm^{-1} for long wavelengths (near 0.25 eV). Again, if doping levels near the active layer are kept at about 10^{17} cm^{-3}, contributions to the mode loss coefficient will be less than 10 cm^{-1}.

In the active layer the worst case is at a wavelength of 5 μm where α/p is 7.4×10^{17} cm^2 for GaAs, 10.4×10^{17} cm^2 for AlSb, and 20.4×10^{17} cm^2 for InAs. If one assumes absorption similar to this data, for 2×10^{18} cm^{-3} at threshold the corresponding values of α in the active layer would be 148, 208 and 400 cm^{-1}. At wavelengths of 2 to 3 μm the values of α should drop by a factor of 5 or so, and thus 30 to 80 cm^{-1} would be the possible range of intervalence band absorption. It should be noted that the intervalence band absorption is only weakly temperature dependent, as seen in Figure 2-14, and would not be greatly improved by operation at low temperatures. As will be shown, for high efficiencies and for successful use of advanced quantum-well structures, the overall mode loss coefficient must be less than about 50 cm^{-1}. The mode loss coefficient for a laser is determined by a weighted average of the free-carrier absorption in all of the layers, where the weighting function is the normalized mode intensity.

2.4.3 Advanced Structures

As mentioned earlier, lower threshold currents have been obtained with GaAs/AlGaAs quantum-well structures than with DH lasers. The most successful of these structures has been the

graded-index separate-confinement heterostructure (GRIN-SCH) laser [21]. The active layer consists of single-quantum-well (SQW) or multiple-quantum-well (MQW) layers, and optical confinement is provided by additional layers of graded-alloy composition. Figure 2-15 is a qualitative comparison of maximum mode gain (with respect to wavelength) vs current density for GRIN-SCH SQW, GRIN-SCH MQW and DH lasers. While gain occurs for the GRIN-SCH SQW laser at much lower currents, it is sublinear with current and tends to saturate. To reach threshold, the gain must equal the loss. If the loss were too high (≥ 50 cm^{-1} for the case in Figure 2-15), then the DH laser would have a lower threshold than the GRIN-SCH SQW laser. For AlGaAs/GaAs structures, thresholds near 0.1 kA/cm^2 have been achieved. For GaInAsP/InP, little significant improvement in threshold had been reported using quantum-well instead of DH structures until quite recently. The recent result [22] at 1.3-μm wavelength was for a GRIN-SCH MQW laser with five wells having a threshold current density of 0.41 kA/cm^2, about one-half the best values obtained for DH lasers. Apparently, it is necessary to use the GRIN-SCH MQW laser, since at 1.3-μm wavelength insufficient gain is available from the GRIN-SCH SQW compared with the loss. Free-carrier absorption is of course more important at 1.3 μm than at ~ 0.85 μm. As this trend continues at longer wavelengths it will become more and more difficult to achieve threshold reduction using quantum-well structures.

A strategy that has been proposed for reducing free-carrier absorption and Auger recombination is the use of strained-layer quantum wells [23]-[25]. Figure 2-16 illustrates the effects of strain on the band structure of III-V alloys. Either tension or compression in the plane of the quantum-well layer can be introduced by deliberately growing the layer with a mismatched lattice constant (elastic deformation). In thin layers (50 to 150 Å is the typical thickness range of quantum-well layers), significant strain can be introduced by lattice mismatch without generation of

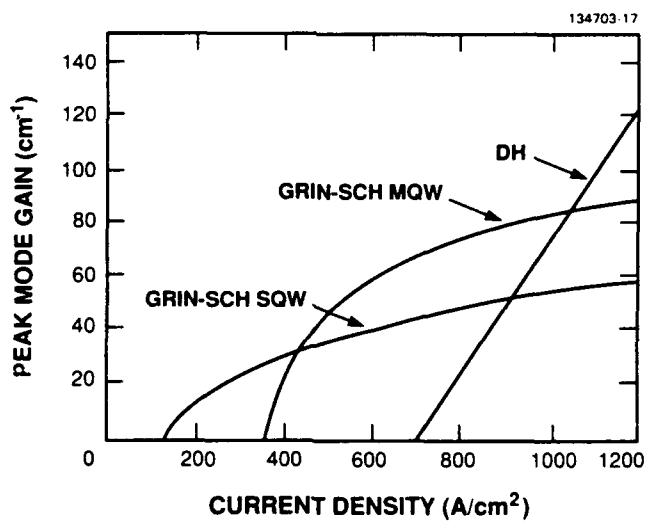

Figure 2-15. Qualitative comparison of peak mode gain vs current density in GaAs/AlGaAs laser structures.

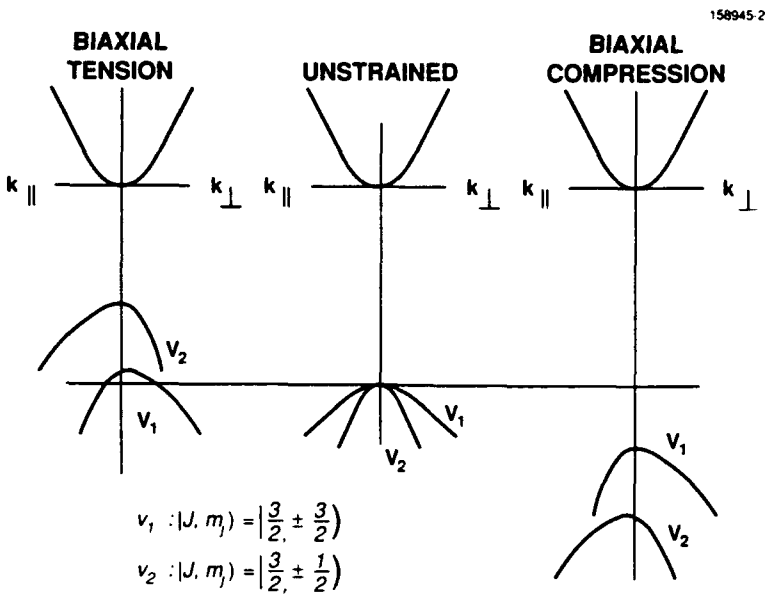

Figure 2-16. Effects of biaxial strain on the valence band structure of III-V semiconductors. Adapted from N.G. Anderson, Ph.D. thesis, North Carolina State University.

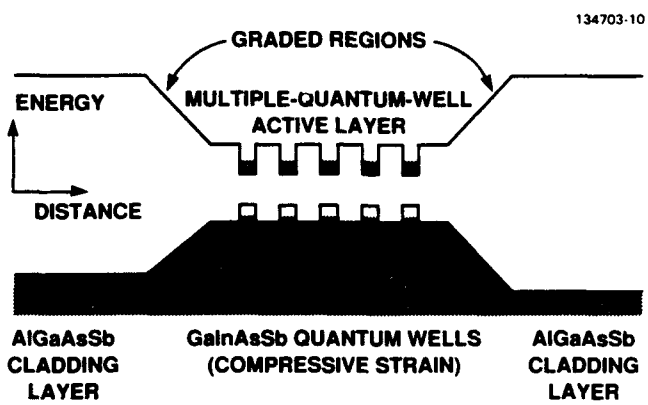

Figure 2-17. Schematic diagram of energy band vs distance for a strained-layer MQW laser. Discrete levels in the wells are not shown. Occupied states under forward-bias conditions are indicated (shaded area).

dislocations (plastic deformation) that in thicker layers relieve the strain and cause electronic defects harmful to laser performance and reliability. As shown in Figure 2-16, the effect of the strain is to remove the degeneracy of the light- and heavy-hole bands at $\mathbf{k} = 0$ and to produce anisotropic effects in a direction $\mathbf{k}_{\parallel}$ parallel to the layer vs the direction $\mathbf{k}_{\perp}$ perpendicular to the layer. The heavy- and light-hole bands are labeled v_1 and v_2, respectively. For the case of compressive strain in the plane of the layer the energy in the v_1 band becomes higher. Figure 2-16 indicates that the mass of the v_1 band in the $\mathbf{k}_{\perp}$ direction is "heavy," but in the $\mathbf{k}_{\parallel}$ direction it becomes "light." The mass in the $\mathbf{k}_{\perp}$ direction determines the discrete quantum levels of the well. However, the mass in the $\mathbf{k}_{\parallel}$ direction determines the density of states in each quantum level and the kinetic energy and momentum of the hole in the free-motion directions of the "two-dimensional gas." According to O'Reilly *et al.* [25], for 1.55-μm lasers the intervalence band absorption can become insignificant for a compressively strained quantum-well structure, while Auger recombination is reduced by a factor of 100 for the CHCC process and by 6 orders of magnitude for the CHSH process. In addition, the smaller density of states that results from the removal of degeneracy reduces the current density needed to produce population inversion, resulting in a lower threshold.

Clearly, it will be important to investigate strained quantum wells for the 2- to 5-μm wavelength range. Figure 2-17 shows the conduction and valence band edges vs distance across the epitaxial layers for a GRIN-SCH MQW structure with strained quantum wells. Ultimately, a structure such as the one in this figure may be required to obtain the desired performance.

A similar structure could be attempted in GaInAsP/InP, where sufficient strain could be incorporated that it should be possible to reach wavelengths in the 2.0 to 2.2-μm range. If there are unexpected problems with the GaInAsSb/AlGaAsSb system this alternative could be attractive. Growth techniques and device fabrication have already been developed significantly in the GaInAsP/InP system for fiber-optic communications applications. As mentioned earlier, attempts to grow quantum-well lasers using that system have met with some limited success recently. However, the system has no potential for longer-wavelength operation. Also, since $\Delta < E_g$ for the GaInAsP/InP system, Auger recombination at longer wavelengths would tend to be a problem if the strained layers are not as effective in reducing this effect as might be expected from optimistic calculations.

2.5 DEVICE PERFORMANCE

The device performance reported for III-V lasers with emission wavelengths beyond 2 μm is summarized in Tables 2-2 and 2-3. Table 2-2 gives results for such lasers fabricated in the GaInAsSb/AlGaAsSb materials system, the system that we find most promising, while Table 2-3 gives results for several other systems.

The GaInAsSb/AlGaAsSb lasers listed in Table 2-2 are DH devices, grown on GaSb substrates, with emission wavelengths of 2.2 to 2.3 μm. The active layer composition is approximately $Ga_{0.84}In_{0.16}As_{0.14}Sb_{0.86}$, and the Al/Ga ratio in the cladding layers ranges from 0.27/0.73 to 0.55/0.45. Room-temperature CW operation has been achieved at both the Lebedev and Ioffe

TABLE 2-2

Device Summary for Diode Lasers with GaInAsSb Active Layer Emitting at 2.2 to 2.3 μm

λ (μm)	T (K)	J_{th} (kA/cm^2)	J_{th}/d (kA/cm^2 μm)	η_d (%)	Cladding Layer $As_xGa_{1-x}As_ySb_{1-y}$ (x)	(y)	Growth	CW at Room Temperature	Authors/ Affiliation	Year
2.2	300	4.2	5.3	-	0.35	0	MBE		Chiu *et al.* [26] AT&T Bell	1986
2.2	290 80	1.7	3.4	5 18	0.4	0.04	LPE		Caneau *et al.* [27] AT&T Bell	1987
2.2	296 80	7 0.6	7.8 0.7	-	0.27	0.02	LPE		Jouille *et al.* [28] Univ. of Languedoc	1988
2.3	300	1.5	-	-	0.55	-	LPE	x	Bochkarev *et al.* [29] Lebedev Institute	1988
2.2	295	5	-	18*	0.34	-	LPE	x	Baranov *et al.* [30] Ioffe Institute	1989
2.2	290 80	2.6 0.1	7.5 0.4	11 20	0.4	0.01	LPE		Zyskind *et al.* [31] AT&T Bell	1989
2.3	295 150	1.7 0.2	4.3 0.5	36	0.5	0.04	MBE		Eglash and Choi [32] Lincoln Laboratory	1990

*Calculated from the light-current characteristic.

TABLE 2-3

Device Summary for 2- to 4-μm Diode Lasers Using III-V Compounds with Active Regions Other Than GaInAsSb

λ (μm)	T (K)	J_{th} (kA/cm^2)	Materials System	Growth	Feature	Authors/ Affiliation	Year
2.4	77 210	0.9 100	InGaAs/ InAsP	Hydride VPE	InP substrate	Martinelli *et al.* [33] David Sarnoff	1989
2.5	50	11	InAsPSb	LPE	-	Akiba *et al.* [34] KDD, Japan	1988
3.0	77 145	3 60	$InAs_{0.94}P_{0.04}Sb_{0.02}$	LPE	-	Kobayashi *et al.* [35] NTT, Japan	1980
3.2	78 110	4.5 13	$InAs_{0.95}Sb_{0.05}$	LPE	InAs substrate	Mani *et al.* [36]	1988
3.9	80	~ 4*	$InAs_{0.91}Sb_{0.09}$/ $Al_{0.5}Ga_{0.5}Sb$	MBE	GaSb substrate	van der Ziel *et al.* [37] AT&T	1986

*Optically pumped.

Institutes for narrow-stripe devices fabricated from laser structures grown by the LPE technique. For broad-stripe devices, pulsed room-temperature values of J_{th} as low as 1.5 kA/cm^2 have been obtained by the Lebedev group, and J_{th} values of 1.7 kA/cm^2 have been obtained at AT&T Bell Laboratories, also for LPE devices, and recently at Lincoln Laboratory for MBE devices. Values of J_{th} of 0.1 and 0.2 kA/cm^2, respectively, have been obtained at 80 K by another group at AT&T Bell Laboratories and at 150 K by the Lincoln Laboratory group. The Lincoln group has achieved the highest room-temperature value of η_d, 36 percent for both facets.

On the basis of these promising results obtained at a number of laboratories, prospects are excellent for the development of GaInAsSb/AlGaAsSb lasers emitting at 2.2 to 2.3 μm that are capable of low-threshold, high-power operation at room temperature. Performance of DH devices should be significantly improved by optimizing the device design—for example, by increasing the Al content of the cladding layers to enhance optical confinement. Using a GRIN-SCH quantum-well structure should lead to still better performance. However, it is unlikely that satisfactory cladding layers with substantially increased Al content can be grown by LPE, because of the difficulty of incorporating sufficient As for lattice matching, and LPE growth of a structure as complex as the GRIN-SCH quantum well would be very difficult. On the other hand, in principle the MBE technique is ideally suited to the growth of complex structures composed of layers with any desired composition. Therefore, the good performance of the Lincoln Laboratory lasers grown by MBE is very encouraging, since it establishes the applicability of MBE to the GaInAsSb/AlGaAsSb system. In particular, the relatively high value of η_d observed for these lasers indicates that the MBE-grown material is of good crystal quality.

As discussed in Section 2.4.1, Sugimura [5] has calculated lower limits of the normalized threshold current density J_{th}/d, where d is the active layer thickness, for DH diode lasers in a number of III-V systems. For convenience in employing Sugimura's results for devices with a GaInAsSb active layer to make comparisons with the experimental data for lasers emitting at 2.2 to 2.3 μm and to make projections for longer wavelengths, we have made a number of simplifying assumptions that permit the use of his calculations to evaluate J_{th}, rather than J_{th}/d. We have assumed that the composition of the cladding layers is $AlAs_{0.08}Sb_{0.92}$, the highest-bandgap AlGaAsSb alloy that is lattice matched to GaSb. Since this alloy is 92-percent AlSb, we can approximate the refractive index n_c of the cladding layers by the refractive index of AlSb, which varies from 3.30 to 3.18 over the wavelength range from 2.0 to 4.5 μm [38]. Over this range, the refractive index n_a varies from 3.77 to 3.67 for GaInAsSb active layers lattice matched to GaSb [39]. Since the difference between n_a and n_c is almost constant, varying only from 0.47 to 0.49, we have used $n_a = 3.72$ and $n_c = 3.24$ in our calculations. By using the condition mentioned earlier from standard guided-wave theory and applying the reasonable criterion that $\Gamma \geq 0.39$, we obtain

$$\frac{\pi d\sqrt{n_a^2 - n_c^2}}{\lambda} \geq 0.5 \ . \tag{2.4}$$

From this expression, $d \geq 0.0871\ \lambda$. We have used this relationship for the minimum value of d together with Sugimura's calculations for DH lasers to obtain the values of J_{th} as a function of

temperature that are shown by the dashed curves plotted in Figure 2-18 for λ= 2, 2.5, 3 and 4 μm. A solid horizontal line is drawn in Figure 2-18 at J_{th} = 20 kA/cm^2, which is about the maximum value of J_{th} that is acceptable for practical device operation.

The experimental data available for comparison with the calculated curves in Figure 2-18 are limited to the results summarized in Table 2-2 for GaInAsSb/AlGaAsSb DH lasers emitting at 2.2 to 2.3 μm. The lowest values of J_{th} at 80, 150 and 295 K from Table 2-2 are plotted in Figure 2-18. In comparison with the values of J_{th} at λ = 2.3 μm obtained by interpolation from the curves for 2 and 2.5 μm, the measured values for 80 and 150 K are about the same. However, the measured value for 295 K, 1.7 kA/cm^2, is lower by a factor of 4 than the interpolated value, even though the actual thickness of the laser active layer was twice the value of d assumed in deriving the curves. This discrepancy indicates that, at least at 2.3 μm, Sugimura's calculations substantially overestimate the probability of Auger recombination, which he found to be the dominant process in determining J_{th} in the vicinity of room temperature. (The better consistency of the experimental and calculated values for 80 and 150 K indicates that the calculations are more accurate for radiative recombination, which is the dominant process at the lower temperatures.) If we assume that Auger recombination is also significantly overestimated for wavelengths beyond 2.3 μm, and also assume that marked improvements in laser operation can be achieved by improving the device structure, particularly by the use of GRIN-SCH quantum-well structures with strained active layers, then the prospects for developing high-performance GaInAsSb/AlGaAsSb lasers for room-temperature operation at longer wavelengths are much brighter than would be concluded on the basis of the calculated curves in Figure 2-18.

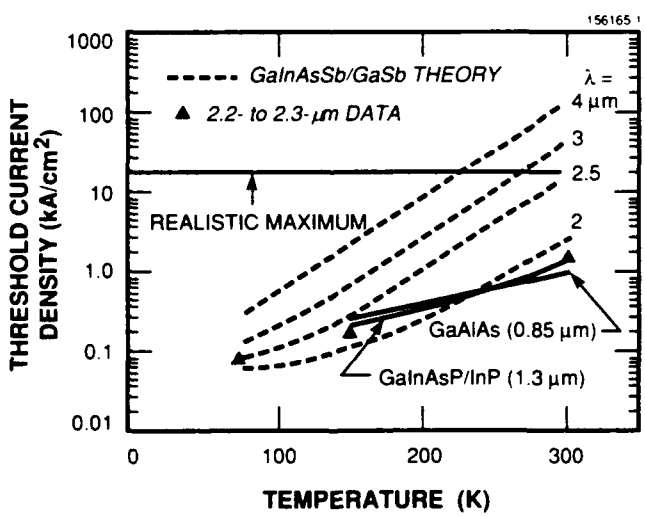

Figure 2-18. Predicted threshold current vs temperature for III-V DH lasers. Experiment points are for selected 2.2- to 2.3-μm data, and solid lines represent trends of the data for 0.85-μm GaAlAs and 1.3-μm GaInAsP lasers.

2.6 RELIABILITY

Semiconductor lasers generally exhibit three major device degradation mechanisms: oxidation of the output facets, catastrophic damage to the output facets and growth of dark regions in the active layer. Oxidation of the output facets due to atmospheric exposure is easily preventable. The facets can be coated with passivating layers of transparent oxides such as Al_2O_3, which prevent the buildup of the opaque native oxide. The origin of catastrophic facet damage in an AlGaAs laser is optical absorption at the facet surface. It is a problem for very large optical fluxes that occur under high-current pulsed operation. The threshold for catastrophic damage is substantially higher for the longer-wavelength GaInAsP/InP lasers and does not appear to cause a reliability problem in that system. For the 2- to 5-μm lasers, at worst it is likely to be a problem only at very high power densities. Dark regions are regions of crystalline defects that exhibit high nonradiative recombination and therefore neither emit light nor provide amplification for the laser. The movement and growth of these regions into the active layer present a serious problem with semiconductor lasers. The movement is caused by the propagation of defects originally present in the substrate or introduced by contamination and damage that occur during growth and processing.

Dark regions grow far more slowly in GaInAsP/InP lasers than in GaAlAs lasers. One possible explanation for this is an alloy hardening effect associated with having alloy constituents with somewhat different atomic radii in random patterns in the lattice, an arrangement that may give some mechanical support and provide resistance to the motion of defects. Another plausible explanation for the slower propagation of dark regions in GaInAsP is the dependence of the propagation rate on the energy gap. The energy required to generate defects for the growth of dark regions must be supplied by recombining electron-hole pairs. The energy of electron-hole pairs is the energy gap of the active medium plus their thermal energy at room temperature of approximately 0.026 eV. GaAs has an energy gap of 1.43 eV at 0.85-μm lasing wavelength whereas GaInAsP has an energy gap of 0.95 eV at 1.3-μm wavelength. Thus, electron-hole pairs have over 50 percent more energy in GaAs than in GaInAsP. Indeed, some of the earliest GaInAsP lasers operated in a CW mode for hundreds and even thousands of hours without degradation, in sharp contrast to the early experience with GaAlAs lasers.

If this argument is correct, then long-wavelength lasers would have even slower rates of degradation. In the 1.3-μm lasers, however, the yield of extremely reliable devices is very low. This may be related to poor quality of the substrates and the growth technologies used. The probability may be relatively high that a major defect is already present in a device before life testing. For this reason extremely high reliability may require significant materials development.

2.7 SUMMARY

The III-V alloy systems include several possible candidates for diode lasers in the 2- to 5-μm wavelength range. Because of its metallurgical properties, its large range of available wavelengths

and its favorable band structure for minimizing Auger recombination ($\Delta > E_g$), GaInAsSb/AlGaAsSb/GaSb is the most promising system.

The estimates of threshold current densities given here for conventional DH lasers are based on the calculations of Sugimura [5]. While Sugimura estimates that his calculations are accurate within a factor of 3, for emission at 2.3-μm wavelength the experimental threshold current densities per micrometer of active layer thickness are nearly 5 times smaller than the calculated values. Hence, Auger recombination may not limit room-temperature operation at longer wavelengths as strongly as the estimates indicate. Nevertheless, both Auger recombination and free-carrier absorption are problems for obtaining good device performance, and these problems become increasingly serious with increasing wavelength. At long wavelengths it will be necessary to utilize separate optical and carrier confinement structures and probably, more specifically, MQW strained-layer devices. Doping levels must be minimized to ~ 10^{17} cm^{-3} or less in the regions in which the optical fields are confined in order to reduce free-carrier absorption in the confining layers. Use of strained layers may help reduce the Auger recombination as well as reduce free-carrier losses in the active layers. With strained layers it should be possible with the GaInAsSb/AlGaAsSb/GaSb system to cover the entire wavelength range out to 5 μm.

More refined calculations of threshold could be made if better data were available on free-carrier absorption and Auger recombination in the specific alloys of interest. Calculations of these effects from first principles are always somewhat suspect in the absence of experimental confirmation. As research continues, experimental results on the materials and devices grown for 2- to 5-μm lasers and the future progress in the technology for growing strained-layer quantum-well devices will be the best indicators of the maximum wavelength at which successful devices can be operated.

3. IV-VI MATERIALS SYSTEMS

3.1 WAVELENGTH VS LATTICE CONSTANT

In principle it is possible to obtain lattice-matched DH lasers using the lead salts PbS, PbSe or PbTe as substrates. Figure 3-1 is a diagram of wavelength vs lattice constant for a PbCdSSe quaternary system that can be lattice matched to PbS. However, this system is of limited usefulness since the solubility of Cd is small [40]. Two other quaternary systems, shown in Figure 3-2, are PbEuSeS and PbEuSeTe using PbSe and PbTe, respectively, as substrates. Both are promising but the PbEuSeS system has several advantages. The PbSe and PbS compounds are stronger materials and less easily damaged than PbTe, the PbSSe alloy system is metallurgically superior to the PbSeTe system, and the effective mass anisotropies are smaller for PbS and PbSe than for PbTe. This latter fact should reduce Auger recombination in the PbEuSSe system more than in the PbEuSeTe system, as discussed below. The high vapor pressures of sulfur and selenium as opposed to tellurium are a disadvantage in MBE growth techniques and hot-wall vapor-phase epitaxy (HWVPE) [41] may be required. Diagrams of wavelength vs lattice constant

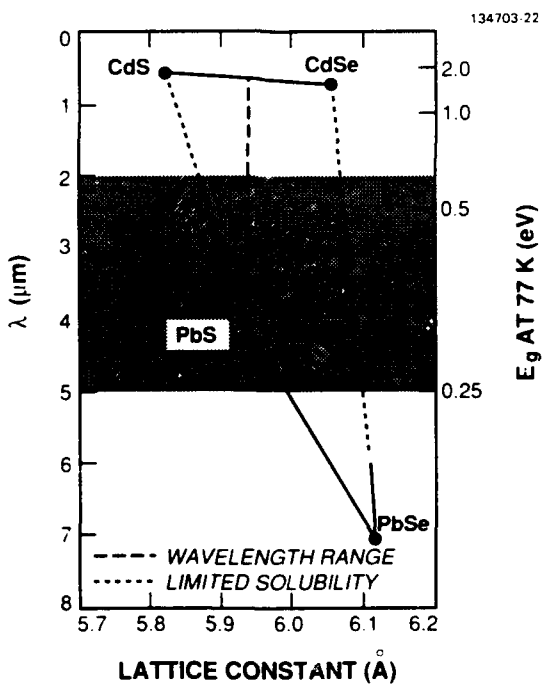

Figure 3-1. Wavelength vs lattice constant for the PbCdSSe quaternary system.

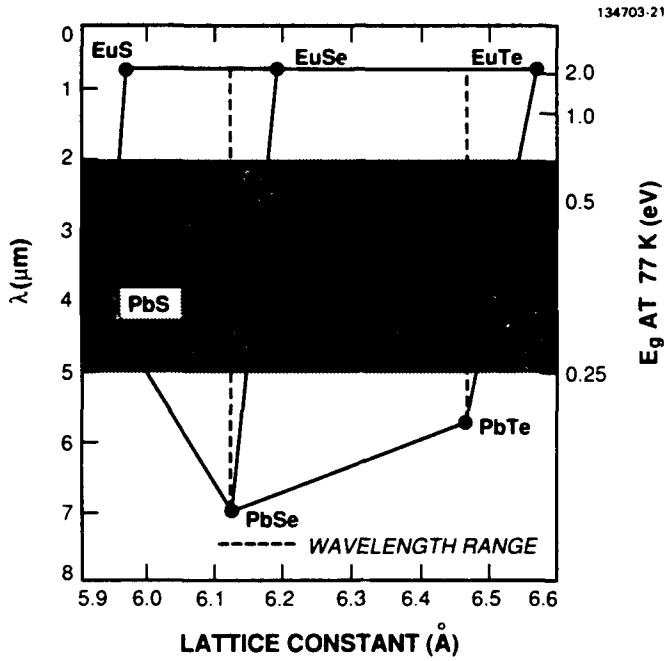

Figure 3-2. Wavelength vs lattice constant for PbEuSSe and PbEuTeSe quaternary systems.

similar to Figure 3-2 can be constructed using Sr, Ca, Ba or Zn, instead of Eu. It is not clear that one is better than another. Recently, PbMnSSe lattice matched to PbS was reported [42], which would have results similar to those in Figure 3-1 and would be likely to present the corresponding solubility problems. It may also be possible to grow a lattice-matched, thermal-expansion-matched $BaSrF_2$ crystal as a transparent, insulating substrate material [43].

3.2 MATERIALS AND GROWTH ISSUES

Bulk Bridgman-grown lead salt materials for substrates can be readily obtained but have dislocation densities in the 10^6- to 10^8-cm^{-2} range. Vapor-grown substrates can be produced with dislocation densities in the range of 10^2 to 10^5 cm^{-2} but are not commercially available. Moreover, it is difficult to cut, grind, polish or otherwise handle lead salt materials without damage, which causes increased dislocation densities. For these reasons, it may be worthwhile to consider $BaSrF_2$ substrates [43] to provide a sturdy backing for the epitaxial layers, giving added damage resistance. However, facets could not be cleaved since the fluorides cleave on (111) planes and the lead salts on (100).

Epitaxial growth by MBE, HWVPE and LPE has been demonstrated [41]. The low growth temperatures permitted by MBE and HWVPE (~ 300 to 400°C) are important since diffusion of electrically active native defects is very rapid. The concentrations of native defects are potentially very large and difficult to control at high temperature. Even at low growth temperatures and with the use of impurity dopants, controlling carrier type and concentration at a level of a few multiples of 10^{17} cm^{-3} may be difficult, although certainly not impossible.

The lead salt materials have several other unattractive features. As shown in Table 2-1 the thermal conductivity of even the binary compounds is very poor. There are many anecdotal instances of unstable device performance due to unstable surfaces, interfaces and contacts. Devices may change their characteristics after sitting a few months at room temperature. Because thermal expansion coefficients are large (see Table 2-1) and devices are easily damaged, it is difficult to cycle lead salt devices in temperature without generating dislocations or even cleaves or cracks. Special mounting, packaging and handling procedures are imperative. Hence, from a materials and growth perspective the lead salts are less attractive than the III-V materials.

3.3 DEVICE PHYSICS

3.3.1 Carrier Mobility

Since the thermal conductivity is already so poor in the IV-VI compounds, it is unlikely that alloy scattering will degrade this parameter significantly. However, there are problems with the electrical conductivity of the alloys. Figure 3-3, which is taken from Partin's recent review paper [44], shows the energy gap vs composition for the PbTe alloys with energy gaps up to about 0.75 eV. These alloys could provide cladding layers with $\Delta E_g \geq 0.4$ eV for wavelengths of 3.5 μm or longer, but the electron mobility at 80 K for the highest E_g alloys is only about 50 cm^2 V^{-1} s^{-1} or less, as shown in Figure 3-3(b), and would degrade further with increasing temperature.

It is likely that the wide-bandgap alloys of PbEuSSe will show similar degradation in mobility. In order to estimate the amount of Eu required for the cladding layer, it is useful to look at the ternary alloy $Pb_{1-x}Eu_xSe$, which is nearly lattice matched to PbSe. In Figure 3-4, the energy gap vs composition is plotted at 300 K and 77 K. This dependence is based on the assumption that the energy gap increases linearly with x. In fact, however, for the telluride data shown in Figure 3-3 the increase is much faster than linear, which appears to be the case for the selenides as well, judging from the only data available ($x = 0.04$ and $E_g = 0.45$ eV at 120 K). The dashed line labeled 120 K is drawn from the energy gap of PbSe at 120 K through the data point. It appears that large gaps for $x < 0.10$ are feasible. Also, if room-temperature operation were attempted at wavelengths longer than 4.3 μm, a PbSnSSe quaternary could be used for the active layer lattice matched to PbSe.

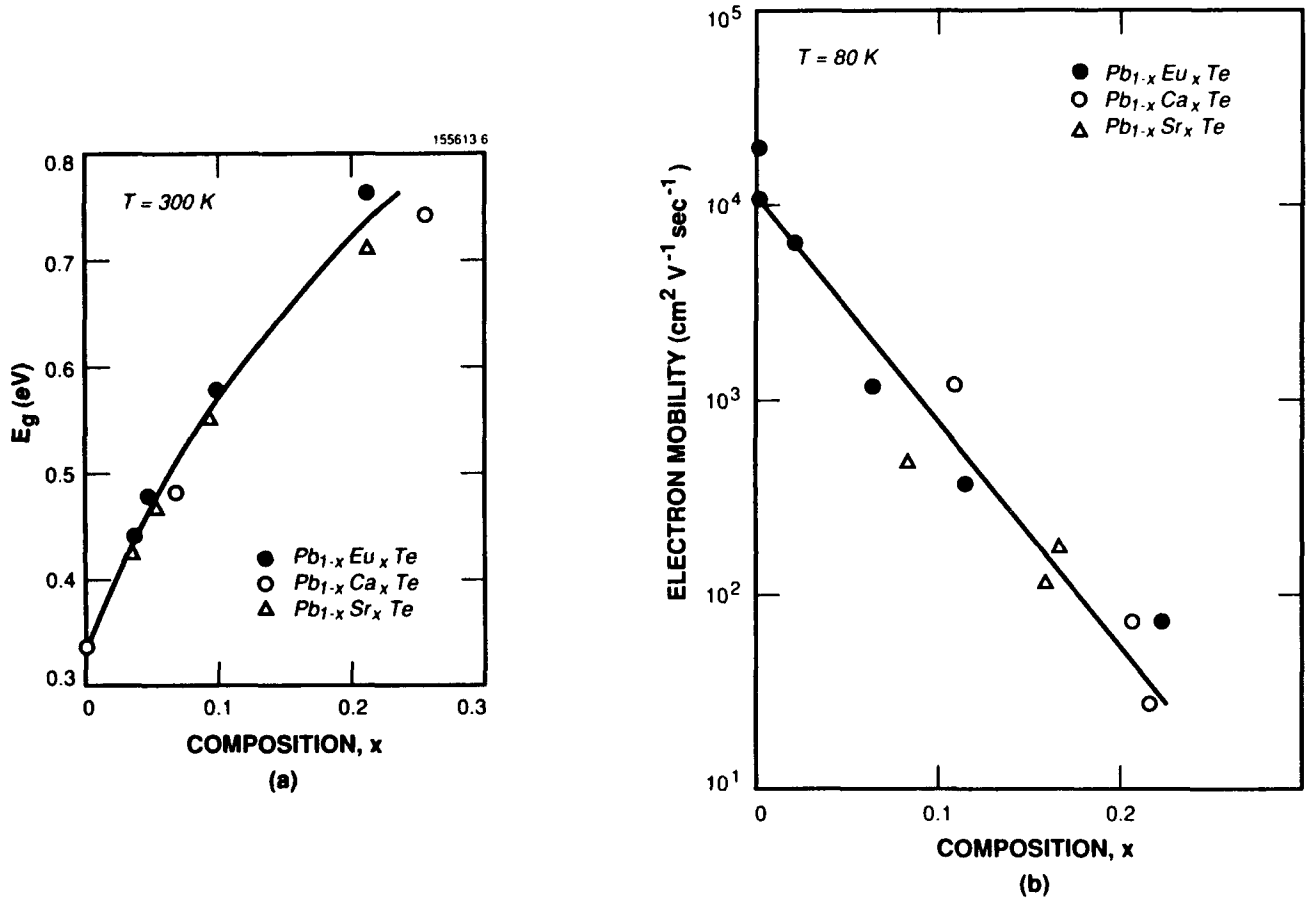

Figure 3-3. Variation of (a) energy gap with alloy composition and (b) electron mobility with alloy composition for some lead salt alloys. Adapted from Partin [44].

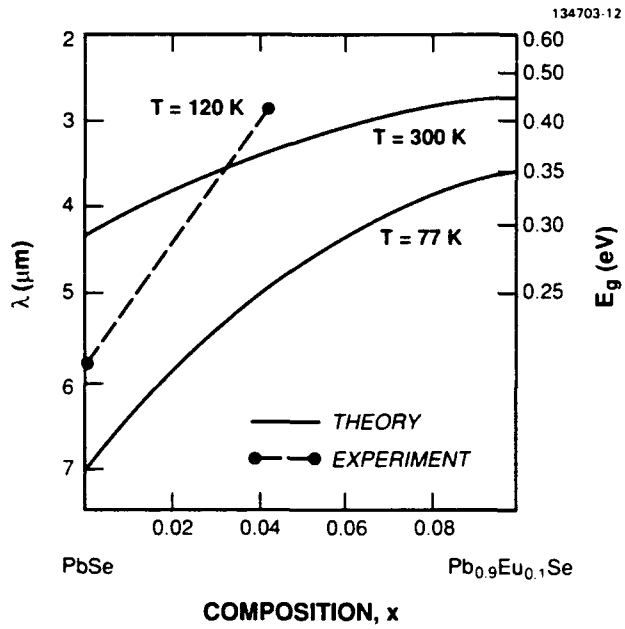

Figure 3-4. Estimated variation of energy gap in the PbEuSe ternary system.

3.3.2 Auger Recombination

Figure 3-5 shows the energy band structure for PbS, which is similar to that for PbSe and presumably for other alloys with small band gaps. The extrema of both the conduction and valence bands occur at the L point. No other extrema are present within at least 1 eV. This situation is highly desirable since it means that Auger recombination and free-carrier absorption will not be enhanced by the effects that occur in the III-V alloys. The Auger rate r_a for carriers in either the conduction or valence bands in the lead salts is, neglecting nonparabolicity, approximately [45]

$$r_a \propto \exp\left(-\frac{rE_g}{2kT}\right), \tag{3.1}$$

where r is equal to m_t/m_l, the ratio of the transverse effective mass to the longitudinal effective mass. Mass anisotropy is a consequence of the location of the band extrema at the L point. For PbSe at room temperature $r \approx 0.5$, so Equation (3.1) becomes

$$r_a \propto \exp\left(-\frac{0.25E_g}{kT}\right). \tag{3.2}$$

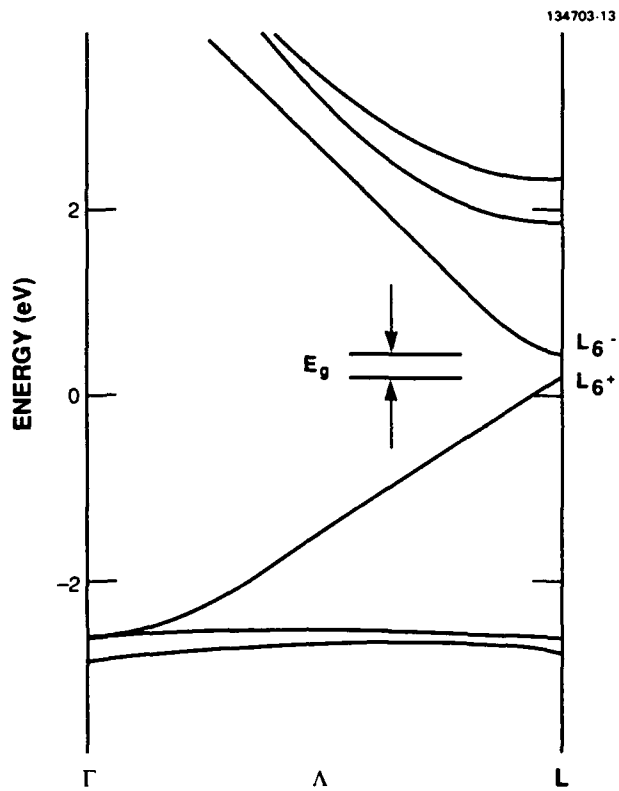

Figure 3-5. PbS energy band structure near the energy gap along the k axis from Γ to L. Position along the k axis is denoted by the group theoretical symbols Γ, Λ and L.

Substituting $\mu = m_C/m_H = 0.1$ in Equation (2.1), which describes the CHCC process, we have

$$r_C \propto \exp\left(-\frac{0.1E_g}{kT}\right). \tag{3.3}$$

If we take as an example $E_g = 0.3$ eV ($\lambda = 4.1$ μm), which is the approximate energy gap of PbSe at room temperature, we have

$$\frac{r_a}{r_C} = \exp\left(-\frac{0.15 \times 0.3}{0.026}\right) = 0.18\ . \tag{3.4}$$

Not only is the r_a/r_C ratio small, but of course the r_S and r_L processes are entirely absent. Another important factor not included in Equation (3.4) is the dependence of the Auger rate [15] on the reciprocal of the square of the material dielectric constant, or the fourth power of the refractive

index. This term accounts for another factor-of-4 reduction in the Auger rate of the IV-VI materials compared with the III-V materials.

3.3.3 Free-Carrier Absorption

Because of the simple band structure of the IV-VI alloys, only the simplest intraband free-carrier absorption process needs to be considered. Figure 3-6 shows experimental [46] hole and electron free-carrier absorption for PbS at 300 K. Similar data [47] obtained for PbTe are independent of carrier type and show a λ^p dependence, where p is approximately 2.2 to 2.5. In the active layer of a laser, where we expect carrier densities around 10^{18} cm^{-3}, the room-temperature absorption in the 4- to 5-μm wavelength range would be of the order of 60 to 100 cm^{-1}. Clearly, efficiency would be low without a separate-confinement structure, but somewhat better than the worst cases estimated for the III-V alloys. In the cladding layers to which the optical mode is confined, free-carrier absorption could be a problem because of the low electron mobility associated with the wide-bandgap alloys. Classic free-carrier absorption varies as $(\mu\, m^{*2})^{-1}$, where μ is the mobility and m^* the effective conductivity mass. For the wide-bandgap alloys, m^* should be large. Moreover, μ will vary much less than it does at 77 K. Nevertheless, it still may decrease an order of magnitude if large Eu content is required. At low temperature (~ 80 K), the free-carrier absorption in the active layer should be insignificant because the mobility is increased by over an order of magnitude. Moreover, the Eu content of the cladding can be smaller at low temperatures.

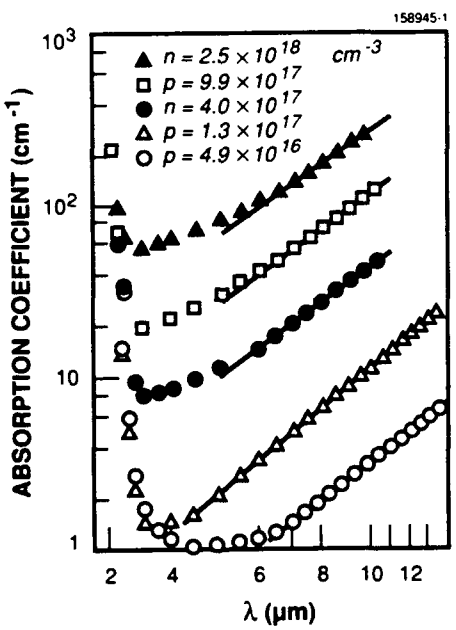

Figure 3-6. Experimental free-carrier absorption in PbS at 300 K.

In Partin's structures [44], the optical mode sees layers with composition $x = 0.02$ and $x = 0.04$, where little reduction in mobility is observed. Even with their small confinement, Partin's structures operate up to 200 K.

3.3.4 Differential Quantum Efficiency

Except at very low temperatures (< 15 K) with homostructure devices, the efficiencies of most lead salt lasers have been very poor. In addition to free-carrier absorption discussed above, explanations that have been offered for this include totally internally reflected modes of oscillation, leakage currents, and nonradiative recombination at dislocations and heterointerfaces. None of these explanations alone explains all the low-efficiency results. Different factors seem to apply to different devices so perhaps the optimum high-efficiency device in which all the problems are eliminated has yet to be fabricated. Nevertheless, the data so far are discouraging.

3.4 DEVICE PERFORMANCE

Some older and more recent benchmark results for lead salt lasers in the wavelength range of interest are summarized in Table 3-1. It should be noted that pulsed operation at 4.4 μm has been achieved in PbSrSe up to 290 K, which is remarkably close to room temperature, but with a very large threshold current density of 400 kA/cm^2.

In Figure 3-7, we modified a graph first presented by Horikoshi [55], showing maximum operating temperature vs wavelength for III-V and IV-VI lasers. For the III-V data we have drawn two straight lines representing a constant product of wavelength and operating temperature, which is expected for an Auger process exponentially varying as $-E_g/kT$. The solid line is positioned to represent all of the III-V data. The dashed line takes into account the best data points for III-V lasers having GaInAsSb active layers. It should be pointed out that no attempts to operate the best 2.3-μm lasers at temperatures above room temperature have been reported. For the IV-VI data we included a curve calculated by Horikoshi [55] for Auger-limited operation. The theory assumes that maximum operating temperature is obtained when the internal quantum efficiency reaches 2.5 percent. The only III-V CW finding shown is the recent result from the Lebedev Institute [26] although CW operation is of course common at shorter wavelengths, namely, $\lambda \approx 0.8$ μm and $\lambda \approx 1.3$ to 1.6 μm. No calculations of threshold current density are available for lead salt lasers in the 2- to 5-μm range, since much of the past work has been on PbTe-based alloys or other long-wavelength materials. To obtain such calculations would require consideration of the radiative and Auger recombination rates and the optical gain at various injected carrier densities. Although the results would be of interest for comparison with Sugimura's work [5] for the III-V material systems, such an undertaking would exceed the scope of this study. Nonetheless, the qualitative trends are apparent and the experimental evidence is in agreement with those trends. As seen in Figure 3-7, the lead salts operate at higher temperatures than the III-V materials at a given

TABLE 3-1

Device Summary for 3- to 5-μm Diode Lasers Using IV-VI Compounds

λ (μm)	T (K)	J_{th} (kA/cm^2)	η_d (%)	Materials System	Growth	Feature	Authors/ Affiliation	Year
2.88	100 CW 120 pulsed	-	-	$Pb_{0.957}Eu_{0.043}Se$	MBE	PbSe substrate	Tacke *et al.* [48] FIPM, Germany	1988
3.25	200	20	-	PbCdSSe/PbS	MBE	PbS substrate	Koguchi *et al.* [49] NRI, Japan	1987
3.45	130	-	-	$Pb_{0.992}Eu_{0.008}Se$	MBE	BaF_2 or PbSe substrate	Norton and Tacke [50] FIPM, Germany	1987
4.1	243 170 CW	30	-	PbEuTe/PbTe	HWE*	PbTe substrate	Nishijima [51] Fujitsu, Japan	1989
4.3	4.2	-	27	PbS	Bulk	P_{out} = 0.35 W	Ralston *et al.* [52] Lincoln Laboratory	1974
4.4	290 169 CW	400	-	PbSrSe/PbSe	MBE	PbSe substrate	Spanger *et al.* [53] FIPM, Germany	1988
6.3	130 CW	4 at 77 K	44	$PbS_{0.03}Se_{0.97}$	CID†	P_{out} = 0.07 W	Linden *et al.* [54] Laser Analytics	1977

* Hot-wall epitaxy.
† Compositional interdiffusion.

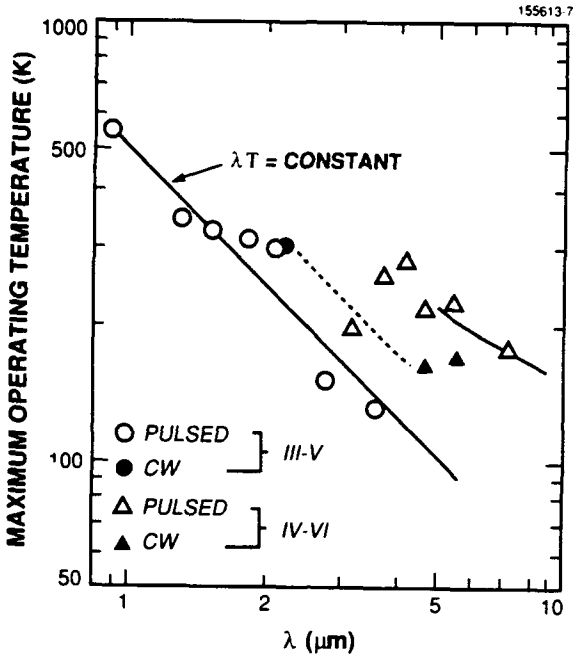

Figure 3-7. Maximum operating temperature vs wavelength for III-V and IV-VI lasers. The solid lines and the dashed line are discussed in the text. Adapted from Horikoshi [55].

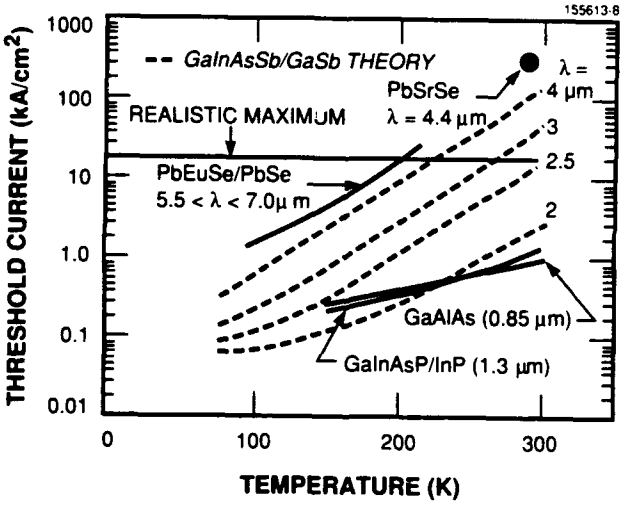

Figure 3-8. Experimental threshold currents vs temperature for some IV-VI lasers compared with III-V predictions.

wavelength as is expected with less severe Auger recombination. In Figure 3-8 we show the highest IV-VI operating temperatures superimposed for comparison on the III-V theoretical calculations presented earlier. The lead salts show slightly better results for $5.5 < \lambda < 7.0$ μm than might be expected for the III-V materials considering the wavelength. The threshold at $\lambda = 4.4$ μm is not as good as might be expected for the III-V materials.

4. II-VI MATERIALS SYSTEMS

4.1 WAVELENGTH VS LATTICE CONSTANT

The HgCdTe pseudobinary alloys have been extensively developed for photodetectors since their energy gaps correspond to wavelengths throughout the infrared region including the 2- to 5-μm region. Figure 4-1 shows wavelength and energy gap vs lattice constant for the HgCdZnTe quaternary system. The HgCdTe compounds may be precisely lattice matched to either CdZnTe or CdTeSe alloys.

4.2 MATERIALS AND GROWTH ISSUES

The II-VI materials systems have some advantages. They form a continuous series of substitutional solid solutions with an unusually small difference in lattice constant between HgTe and CdTe of 0.3 percent, and there are no miscibility gaps in either the ternary HgCdTe or the quaternary HgCdZnTe alloys. In addition, the lattice-matched substrates CdZnTe and CdTeSe are available, and the applicable growth technologies include LPE, MBE and OMVPE.

Unfortunately, however, the development of light-emitting structures of the HgCdTe alloys has been impeded by relatively high Hg vapor pressure, high atomic diffusion coefficients, and

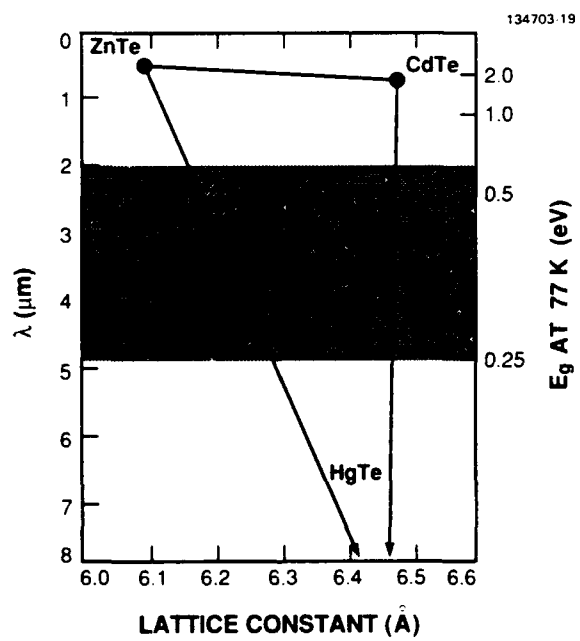

Figure 4-1. Wavelength vs lattice constant for the HgCdZnTe quaternary system.

amphoteric doping behavior for slow-diffusing donor and acceptor impurities. These problems persist for all epitaxial growth methods, including LPE, OMVPE and MBE, although some progress has been reported. Namely, a Te-rich LPE growth process has been developed [56] whereby Sb-doped layers are prepared with 77 K *p*-type carrier concentrations ranging from 1.8×10^{16} to 1.3×10^{19} cm^{-3} for values of x ranging from 0.23 to 0.29. The results represent a step forward toward developing the capability of obtaining HgCdTe multilayer structures with impurity-controlled carrier type and concentration for each layer of the structure. In addition, the II-VI materials like the IV-VI systems have large stoichiometric defect concentrations and poor thermal conductivity (see Table 2-1).

4.3 DEVICE PERFORMANCE

The results that have been obtained with II-VI optical emission devices are summarized in Table 4-1. Melngailis and Strauss [57] observed laser action at 3.8 and 4.1 μm in bulk HgCdTe

TABLE 4-1

Device Summary for Diode Lasers Using II-VI Compounds

λ (μm)	T (K)	Materials System	Feature	Authors	Year
3.0-4.1	10	HgCdTe	Pumped using GaAs diode laser	Melngailis and Strauss [57]	1966
3.7	10	HgCdTe	Spontaneous emission from *p-n* junction	Verie and Granger [58]	1965
2.7	77	HgCdTe/ CdTeSe	Optical pumping (low threshold)	Harman [59]	1980
3.2-4.2	300	HgCdTe	LED with 9.2% efficiency	Tarry [60]	1986
2.5	77	HgCdTe/ $CdTe/Al_2O_3$	LED with 17% internal efficiency	Zucca *et al.* [61]	1988
5.3	77	HgMnTe	Diode laser (J_{th} = 1.3 kA/cm^2)	Becla [62]	1988

crystals excited optically by radiation from a GaAs diode laser at 10 K. Although spontaneous emission [58] from HgCdTe *p-n* junctions has also been observed, no successful work has so far been reported for diode lasers. Pulsed laser emission of 2.7-μm wavelength at 77 K was obtained [59] using LPE-grown HgCdTe layers on CdTeSe substrates optically pumped by a Nd:YAG laser. However, the estimated equivalent laser threshold current was lower than that observed in optically pumped InSb and InAs. HgCdTe light-emitting diodes fabricated from bulk-grown crystals have been reported [60] operating in the 3.2- to 4.2-μm range at room temperature, with efficiencies as high as 0.2 percent and spectrum widths of 0.3 μm. In another study [61] an *n*-type region was formed by ion implantation on a *p*-type HgCdTe layer grown by LPE on a sapphire substrate having a thin CdTe buffer layer grown by OMVPE; a light-emitting diode with a 17-percent internal quantum efficiency at 2.5 μm at 77 K was fabricated from the structure. Also, a 5.3-μm diode laser operating at 77 K has been reported using the $Hg_{1-y}Mn_yTe$ alloy [62].

5. BEAM QUALITY

The geometry of conventional single-stripe diode lasers in the AlGaAs/GaAs and GaInAsP/InP materials systems imposes a limitation on the output power that can be achieved while maintaining good beam quality. These same limitations will apply to longer-wavelength diode lasers and will impose an even more stressing trade-off between beam quality and output power.

The most straightforward way to achieve a good-quality, stable beam from a diode laser is to fabricate an index-guided, cleaved-facet structure with a sufficiently narrow stripe that the waveguide operates in a single lateral mode. Any astigmatism can be readily compensated by the appropriate anamorphic collection optics to yield a near-diffraction-limited circular output beam. However, the necessity of using a narrow stripe means that the output power from such a device is limited either by current leakage and other parasitic effects or, more fundamentally, by heating at high current drive levels. High power from a narrow stripe also implies high optical power density. Catastrophic facet damage is the result of optical absorption at the laser output facets. It is known to be a problem for very large optical fluxes that occur under high-current pulsed operation of AlGaAs/GaAs lasers. The threshold for catastrophic damage is substantially higher for the longer-wavelength GaInAsP/InP lasers. The extent of the problem to be expected in the 2- to 5-μm lasers is unknown, but it is not likely to be any worse than for AlGaAs/GaAs lasers.

The biggest difficulty with obtaining high power from 2- to 5-μm lasers will be thermal limits. The relatively high thresholds and low differential quantum efficiencies anticipated for 2- to 5-μm lasers mean that the wall-plug efficiencies of these lasers will be substantially lower than those observed for shorter-wavelength lasers. Correspondingly, the heat generated will be much higher at the same optical output power. Because laser performance degrades at high temperatures, output power as a function of injection current reaches a maximum and then declines. For narrow-stripe GaInAsP/InP lasers, the maximum CW power is typically in the range of a few tens of milliwatts. This maximum will be lower for 2- to 5-μm narrow-stripe lasers and may well be in the range of a few milliwatts and therefore inadequate for the intended applications.

Power levels can be increased by employing lasers with stripes that are much wider than required for single-lateral-mode operation. In such lasers the current density needed for a given total output power is reduced, and the thermal load is spread over a wider area allowing better heat extraction. However, wide-stripe lasers usually have poor-quality, unstable beams. Improvement of beam quality in high-power, wide-stripe lasers has been sought through three approaches: the use of (1) multiple-coupled-stripe structures, (2) external-cavity-stabilized lasers and (3) wide-stripe structures operated as power amplifiers.

In the first approach, guiding (or antiguiding) stripe structures are fabricated within the wide stripe to control the lateral mode to yield a stable output beam that can be optically transformed into a near-diffraction-limited circular beam. However, experiments to date, primarily in AlGaAs/GaAs structures, indicate that the difficulty controlling the lateral mode increases with the number of

guides and with the stripe width. Even with higher efficiency lasers, diffraction-limited beams at output powers above 1 W have been difficult to achieve. Recent work on AlGaAs/GaAs antiguiding multiple-stripe structures has yielded stable beams for as many as 40 coupled stripes. These promising results indicate that work on antiguiding arrays in 2- to 5-μm lasers may well yield a few watts of output power with a reasonable quality of the beam.

The second approach to extracting high-power, diffraction-limited beams from wide-stripe diode lasers is to operate the laser in an external cavity where the optical elements of the cavity stabilize the lateral mode. This approach has been explored at Lincoln Laboratory and at other institutions. To date, diffraction-limited beams have been achieved for AlGaAs/GaAs lasers at powers of less than 1 W, and technological improvements may well yield good beam quality at levels of several watts CW. However, the low efficiency of 2- to-5-μm diode lasers is likely to limit the output power of a wide-stripe laser to less than 1 W. Also, thermal distortions in a wide-stripe laser will limit the capacity of external optics to stabilize the lateral mode of the laser. Therefore, beam quality is likely to degrade for power over 1 W.

The third technique for obtaining high-quality output beams from a wide-stripe laser is to operate the laser as an injection-locked laser or power amplifier. In this case, the output beam usually retains the spectral and spatial qualities of the injecting laser, which at low laser power can be quite good. However, as the power level out of the amplifier laser increases, thermal distortions degrade the beam quality, and parasitic self-oscillations occur. Thus, for AlGaAs/GaAs power amplifiers, the power consistent with near-diffraction-limited beams has generally been limited to less than 1 W. The longer-wavelength lasers should not be expected to exceed this performance.

It seems likely that the maximum output power in a diffraction-limited beam from any single-stripe, long-wavelength laser will be less than 1 W. If this is true, many lasers must be operated in parallel to achieve the desired multiwatt output. Laser arrays can be configured to optimize the efficiency of individual lasers and subsequently spread out adequately to dissipate the heat generated. Then, the challenge is to coherently combine the output of the lasers into a narrow beam. There are two basic approaches for achieving diffraction-limited beams from arrays of discrete lasers. The first is to operate each laser at a different wavelength and then combine the outputs with a series of dichroic beam splitters. Because high spectral quality is not necessary for the intended applications, this approach is, in principle, feasible. However, the required optical system with a dichroic mirror matched to the wavelength of each laser is likely to be very cumbersome. The other approach is to operate all the lasers coherently, lock the phase relationship of each laser in a predetermined pattern, and then coherently add the output of all the lasers. Many different approaches for coherent operation of diode laser arrays have been pursued at a number of laboratories including several large efforts in recent years supported by AFWL involving AlGaAs/GaAs diode laser arrays.

One approach to coherently operating laser arrays is to place a number of AlGaAs/GaAs laser sections end-to-end, couple the lasers to each other by waveguides between the lasers, and then place gratings over the waveguides to provide both frequency-selective feedback to the lasers and

coupling of the light out perpendicular to the wafer. This approach yields a high degree of temporal coherence, but combining the outputs into a single beam remains a challenge. The basic technique should be extendable to longer-wavelength devices provided that the efficiency obtained is sufficiently high that the laser sections can be placed in close proximity without exceeding a tolerable thermal level.

A second approach is to employ a master oscillator and then distribute the output from this oscillator to a linear array of laser amplifiers by means of a number of optical waveguides and splitters. Stacks of linear amplifier arrays are employed. The output from each edge-emitting amplifier is collimated by fill optics. An external wavefront analyzer measures the quality of the output beam and provides feedback signals to a phase shifter associated with each amplifier. The feedback control establishes the proper phase relationship between the amplifier outputs to combine them into a single beam. Formation of the optical signal-distribution system remains a major challenge of this approach. The technique should be extendable to longer wavelengths, but the lower efficiencies of the longer-wavelength amplifiers and injected waveguides could make the technique difficult to apply.

A third approach is to operate an array of antireflection-coated lasers as gain elements in an external cavity. Fill optics collimates the output of each laser. Feedback to each laser and from one laser to another is provided by a partially reflecting mirror on the opposite side of the cavity from the lasers. Elements such as spatial or Talbot-plane filters are placed in the cavity to lock the laser outputs in the proper phase relationship to yield a single output beam. The feasibility of this technique has been demonstrated both at 0.89 μm with AlGaAs/GaAs diode laser arrays and at 1.3 μm with GaInAsP/InP diode laser arrays. At the longer wavelength, the tendency of the lasers to operate in multiple longitudinal modes makes coherent operation of the laser more difficult. This problem may be exacerbated in the > 2-μm lasers. However, the detailed physics of these devices is still unclear so it is premature to assess the tendency toward multimode operation. In principle, the external-cavity technique is extendable to longer wavelengths.

A fourth approach employs phase conjugation or four-wave mixing. In the absence of some means for locking the phase relationship between the outputs of the laser in a distributed array, the output beam will have poor quality, i.e, it will be many times diffraction limited. Phase conjugation provides a way to extract the energy from a poor-spatial-quality, high-power optical beam and convert the power into a high-quality, high-power output beam. Techniques of this general type have been employed with arrays of 0.8-μm AlGaAs/GaAs lasers. However, the techniques will not be extendable to longer wavelengths because photorefractive materials and other phase-conjugation media have rapidly declining response at wavelengths > 1 μm.

Despite the considerable effort in developing these techniques for coherent operation of arrays of diode lasers, the best approach is still not clear. To date, no laboratory has achieved over 1 W in a diffraction-limited beam although the approaches appear in principle to be capable of substantially higher power levels. As successful techniques for operation of coherent arrays are

developed, it is likely that adaptations of these techniques will be necessary to achieve multiwatt output powers from diode laser arrays in the 2- to 5-μm wavelength range.

6. SUMMARY AND CONCLUSIONS

Among the III-V materials systems, GaInAsSb/AlGaAsSb/GaSb looks very promising from a materials perspective. Good quality GaSb substrates are available, and epitaxial growth does not present any obvious problems. However, from the point of view of device physics the system has two major limitations: Auger recombination may limit operation at room temperature for DH lasers to less than about 3-μm wavelength, and free-carrier absorption limits efficiency at any wavelength. Short wavelength operation is hurt by intervalley conduction band absorption in the active layer and the *n*-type cladding layer. Long wavelength efficiency suffers from light-to-heavy-hole intervalence band absorption in the active and *p*-type cladding layers. These processes are not dependent on carrier scattering mechanisms and hence do not strongly decrease with temperature as does classic intravalley free-carrier absorption. Therefore, advanced structures are needed to optimize bandgap variations and doping levels in separate-confinement structures. Strained-layer quantum wells, in particular, may provide significant improvement.

Auger recombination will be less of a problem in the IV-VI systems than in the III-V systems. Also, free-carrier absorption should in principle have a smaller effect on efficiency, especially at low temperatures. However, observed efficiencies in the IV-VI systems have been poor and this has not been adequately accounted for. In addition, it may be difficult to both maintain good electrical mobility and obtain the large confinement required to operate at room temperature. Furthermore, special handling techniques will be required to obtain good quality substrates since material properties and epitaxial growth are relatively poor. Thermal conductivity, for example, is much worse in the IV-VI than the III-V alloys. The lead salt systems, particularly PbEuSSe/PbSe or a similar one, have potential in the 3.5- to 5-μm range for operation above 200 K. However, major materials development would be required and reliability would be a problem.

At present there is no fundamental basis for either accepting or rejecting the HgCdTe alloys for 2- to 5-μm diode lasers. Research and development progress in the II-VI materials system has been slow, primarily because of the difficult problems associated with the materials technology, although some advances have recently been made. Another difficulty with the II-VI alloys is that they have the same band structure as the III-V alloys and thus have similar problems of Auger recombination and free-carrier absorption. From what is known this system has no advantages and should be eliminated from consideration except for very long term development.

Based on these considerations, we conclude that the best option for laser operation at 2- to 2.5-μm wavelength at room temperature, and at 3.5- to 4.2-μm wavelength at 80 to 200 K, is the GaInAsSb/AlGaAsSb/GaSb system. Separate-confinement quantum-well lasers and strained-layer quantum wells should be developed to operate at long wavelengths at room temperature and to improve efficiency. Designing the optimum device will require consideration of all factors and accurate knowledge of fundamental parameters, particularly electron mobilities and free-carrier absorption coefficients of various alloys. Minimizing electrical resistance vs free-carrier absorption

will be among the necessary compromises. Also, unless strained layers are used, III-V laser operation in the 4.5- to 5-μm range will require a ternary substrate since no binary exists for lattice matching to these alloys.

We recommend proceeding with development of III-V lasers, including the advanced structures discussed in Section 2. The lead salts are a second choice for lasers operating in the 4.5- to 5-μm range if major problems with the III-V materials become apparent.

REFERENCES

1. H.C. Casey, Jr. and M.B. Panish, *Heterostructure Lasers, Part A: Fundamental Principles* (Academic, New York, 1978), pp. 245-253.
2. C. Caneau, J.L. Zyskind, J.W. Sulhoff, T.E. Glover, J. Centanni, C.A. Burrus, A.G. Dentai, and M.A. Pollack, *Appl. Phys. Lett.* **51**, 764 (1987).
3. R.A. Swalin, *Thermodynamics of Solids* (Wiley, New York, 1972), p. 194.
4. T.H. Chiu, J.L. Zyskind, and W.T. Tsang, *J. Electron. Mater.* **16**, 57 (1987).
5. A. Sugimura, *IEEE J. Quantum Electron.* **QE-18**, 352 (1982); *IEEE J. Quantum Electron.* **QE-17**, 627 (1981).
6. A.R. Beattie and P.T. Landsberg, *Proc. R. Soc. (London)* **A-249**, 16 (1959).
7. I. Mito, M. Kitamura, K. Kobayashi, S. Murata, M. Seki, Y. Odagiri, H. Nishimoto, M. Yamaguchi, and K. Kobayashi, *J. Lightwave Technol.* **LT-1**, 195 (1983).
8. H.Y. Fan, in *Semiconductors and Semimetals*, edited by R.K. Willardson and A.C. Beer (Academic, New York, 1967), Vol. 3, p. 406.
9. W.G. Spitzer and J.M. Whelan, *Phys. Rev.* **114**, 59 (1959).
10. I. Balslev, *Phys. Rev.* **173**, 762 (1968).
11. W.P. Dumke, M.R. Lorenz, and G.D. Pettit, *Phys. Rev. B* **1**, 4668 (1970).
12. W.M. Becker, A.K. Ramdas, and H.Y. Fan, *J. Appl. Phys.* **32**, 2094 (1961).
13. M.R. Lorenz, J.C. McGroddy, T.S. Plaskett, and S. Porowski, *IBM J. Res. Dev.* **13**, 583 (1969).
14. S.J. Eglash and K.A. McIntosh, unpublished.
15. B.K. Ridley, *Quantum Processes in Semiconductors* (Clarendon, Atlanta, Ga., 1988), p. 27.
16. R. Braunstein and E.O. Kane, *J. Phys. Chem. Solids* **23**, 1423 (1962); R. Braunstein, *J. Phys. Chem. Solids* **8**, 280 (1959).
17. H.C. Casey and P.L. Carter, *Appl. Phys. Lett.* **44**, 82 (1984).
18. C.H. Henry, R.A. Logan, F.R. Merritt, and J.P. Luongo, *IEEE J. Quantum Electron.* **QE-19**, 947 (1983).
19. J.D. Wiley and M. DiDomenico, Jr., *Phys. Rev. B* **3**, 375 (1971).
20. F. Matossi and F. Stern, *Phys. Rev.* **111**, 472 (1958).
21. W.T. Tsang, *Appl. Phys. Lett.* **39**, 134 (1981).

22. A. Kasukawa, Y. Imajo, I.J. Murgatroyd, and S. Kashiwa, *Conf. Lasers Electro-Optics Tech. Dig.* (Optical Society of America, Washington, D.C., 1989), Paper TuD3.

23. A.R. Adams, *Electron. Lett.* **22**, 249 (1986).

24. E. Yablonovitch and E.O. Kane, *J. Lightwave Technol.* **LT-4**, 504 (1986).

25. E.P. O'Reilly, K.C. Heasman, A.R. Adams, and G.P. Witchlow, *Superlatt. Microstruct.* **3**, 99 (1987).

26. T.H. Chiu, W.T. Tsang, J.A. Ditzenberger, and J.P. van der Ziel, *Appl. Phys. Lett.* **49**, 1051 (1986).

27. C. Caneau, J.L. Zyskind, J.W. Sulhoff, T.E. Glover, J. Centanni, C.A. Burrus, A.G. Dentai, and M.A. Pollack, *Appl. Phys. Lett.* **51**, 764 (1987); *11th IEEE Int. Semiconductor Laser Conf.* (IEEE, New York, 1988), Paper E-4.

28. A. Jouillie, C. Alibert, H. Mani, F. Pitard, E. Tournie, and G. Boissier, *Electron. Lett.* **24**, 1076 (1988).

29. A.E. Bochkarev, L.M. Dolginov, A.E. Drakin, P.G. Eliseev, and B.N. Sverdlov, *Sov. J. Quantum Electron.* **18**, 1362 (1988).

30. A.N. Baranov, A.N. Imenkov, M.P. Mikhailova, A.A. Rogachev, and Y.P. Yakovlev, *Proc. SPIE* **1048**, 188 (1989).

31. J.L. Zyskind, J.C. DeWinter, C.A. Burrus, J.C. Centanni, A.G. Dentai, and M.A. Pollack, *Electron. Lett.* **25**, 568 (1989).

32. S.J. Eglash and H.K. Choi, submitted to *Appl. Phys. Lett.*

33. R.U. Martinelli, T.J. Zamerowski, and P.A. Longeway, *Appl. Phys. Lett.* **54**, 277 (1989).

34. S. Akiba, Y. Matsushima, T. Iketani, and M. Usami, *Electron. Lett.* **24**, 1069 (1988).

35. N. Kobayashi and Y. Horikoshi, *Jpn. J. Appl. Phys.* **19**, L641 (1980).

36. H. Mani, A. Joullie, G. Boissier, E. Tournie, F. Pitard, A.-M. Joullie, and C. Alibert, *Electron. Lett.* **24**, 1542 (1988).

37. J.P. van der Ziel, T.H. Chiu, and W.T. Tsang, *Appl. Phys. Lett.* **48**, 315 (1986).

38. B.O. Seraphin and H.E. Bennett, in *Semiconductors and Semimetals*, edited by R.K. Willardson and A.C. Beer (Academic, New York, 1967), Vol. 3, p. 499.

39. M.L. Dolginov, A.E. Drakin, L.V. Druzhinina, P.G. Eliseev, M.G. Mil'vidskii, B.N. Sverdlov, and V.A. Skripkin, *J. Soviet Laser Res.* **5**, 349 (1984).

40. A.R. Calawa, J.A. Mroczkowski, and T.C. Harman, *J. Electron. Mater.* **1**, 191 (1972).

41. H. Preier, *Appl. Phys.* **20**, 189 (1979); Y. Nishijima, *J. Appl. Phys.* **65**, 935 (1989).

42. N. Koguchi, S. Takahashi, and T. Kiyosawa, *Jpn. J. Appl. Phys.* **27**, L2376 (1988).

43. R.H. Nafziger, *J. Am. Ceram. Soc.* **54**, 467 (1971); R.C. Pastor and A.C. Pastor, *Mater. Res. Bull.* **11**, 1043 (1976).

44. D.L. Partin, *IEEE J. Quantum Electron.* **24**, 1716 (1988).

45. P.R. Emtage, *J. Appl. Phys.* **47**, 2565 (1978); G.P. Agrawal and N.K. Dutta, *Long-Wavelength Semiconductor Lasers* (Van Nostrand Reinhold, New York, 1986), p. 442.

46. T.C. Harman and A.J. Strauss, *J. Electron. Mater.* **5**, 621 (1976).

47. A.J. Strauss, *J. Nonmet.* **1**, 133 (1973).

48. M. Tacke, B. Spanger, A. Lambrecht, P.R. Norton, and H. Bottner, *Appl. Phys. Lett.* **53**, 2260 (1988).

49. N. Koguchi, T. Kiyosawa, and S. Takahashi, *J. Cryst. Growth* **81**, 400 (1987).

50. P. Norton and M. Tacke, *J. Cryst. Growth* **81**, 405 (1987).

51. Y. Nishijima, *J. Appl. Phys.* **65**, 935 (1989).

52. R.W. Ralston, J.N. Walpole, A.R. Calawa, T.C. Harman, and J.P. McVittie, *J. Appl. Phys.* **45**, 1323 (1974).

53. B. Spanger, U. Schiessl, A. Lambrecht, H. Bottner, and M. Tacke, *Appl. Phys. Lett.* **53**, 2582 (1988).

54. K.J. Linden, K.W. Nill, and J.F. Butler, *IEEE J. Quantum Electron.* **QE-13**, 720 (1977).

55. Y. Horikoshi, in *Semiconductors and Semimetals*, edited by R.K. Willardson and A.C. Beer (Academic, New York, 1967), Vol. 2, p. 93.

56. T.C. Harman, to be published.

57. I. Melngailis and A.J. Strauss, *Appl. Phys. Lett.* **8**, 179 (1966).

58. C. Verie and R. Granger, *Compt. Rend. Acad. Sci. Paris* **261**, 3349 (1965).

59. T.C. Harman, *J. Electron. Mater.* **8**, 191 (1979).

60. H.A. Tarry, *Electron. Lett.* **22**, 416 (1986).

61. R. Zucca, J. Bajaj, and E.R. Blazejewski, *J. Vac. Sci. Technol. A* **6**, 2728 (1988).

62. P. Becla, *J. Vac. Sci. Technol. A* **6**, 2725 (1988).

REPORT DOCUMENTATION PAGE

Form Approved
OMB No. 0704-0188

Public reporting burden for this collection of information is estimated to average 1 hour per response, including the time for reviewing instructions, searching existing data sources, gathering and maintaining the data needed, and completing and reviewing the collection of information. Send comments regarding this burden estimate or any other aspect of this collection of information, including suggestions for reducing this burden, to Washington Headquarters Services, Directorate for Information Operations and Reports, 1215 Jefferson Davis Highway, Suite 1204, Arlington, VA 22202-4302, and to the Office of Management and Budget, Paperwork Reduction Project (0704-0188), Washington, DC 20503

1. AGENCY USE ONLY *(Leave blank)*	2. REPORT DATE	3. REPORT TYPE AND DATES COVERED
	22 August 1990	Technical Report 1 November 1988 — 30 September 1989

4. TITLE AND SUBTITLE

Materials Systems for 2- to 5-μm Wavelength Diode Lasers

5. FUNDING NUMBERS

C — F19628-90-C-0002

6. AUTHOR(S)

J.N. Walpole, T.C. Harman,
S.H. Groves, R.C. Williamson, and A.J. Strauss

7. PERFORMING ORGANIZATION NAME(S) AND ADDRESS(ES)

Lincoln Laboratory, MIT
P.O. Box 73
Lexington, MA 02173-9108

8. PERFORMING ORGANIZATION REPORT NUMBER

TR-898

9. SPONSORING/MONITORING AGENCY NAME(S) AND ADDRESS(ES)

WL/AROF
Kirtland AFB, NM 87117-6008

10. SPONSORING/MONITORING AGENCY REPORT NUMBER

ESD-TR-90-066

11. SUPPLEMENTARY NOTES

None

12a. DISTRIBUTION/AVAILABILITY STATEMENT

Approved for public release; distribution is unlimited.

12b. DISTRIBUTION CODE

13. ABSTRACT *(Maximum 200 words)*

Several materials systems are reviewed in an attempt to determine the most favorable for use in the fabrication of diode lasers emitting in the 2- to 5-μm wavelength range. Eight possible systems, along with several of their variations, are identified among the III-V, IV-VI and II-VI semiconductors. All meet the following criteria: optical and carrier confinement can be obtained, a significant portion of the desired wavelength range can be achieved, and the layers that are required to fabricate a double-heterostructure (DH) laser can be lattice matched to a suitable substrate.

The performance of III-V laser devices is limited by Auger recombination and free-carrier absorption. The role of the valence band structure in these effects is of particular importance. The III-V system identified as the most promising is GaInAsSb/AlGaAsSb/GaSb, with the quaternary alloy GaInAsSb for the active layer, the quaternary alloy AlGaAsSb for the cladding layers, and GaSb for the substrate. This system offers substrate availability, a wide range of wavelengths, good metallurgical properties and favorable device physics. In this system, DH lasers emitting at ~2.3 μm have been operated CW at room temperature with threshold current densities as low as 1.5 A/cm^2, and differential quantum efficiencies as high as 18 percent per facet have been obtained in pulsed room-temperature operation. According to theoretical projections, the threshold current density of such GaInAsSb/AlGaAsSb/GaSb lasers will increase with increasing wavelength because of increased Auger recombination and free-carrier absorption. In order to reduce these effects and generally improve device performance, we recommend that strained-layer quantum-well devices be investigated.

The IV-VI systems in principle should have less Auger recombination than the III-V systems, as well as less free-carrier absorption, because of the simpler valence band structure of IV-VI materials compared with that of III-V materials. Nevertheless, these effects remain important and limit performance. In addition, the IV-VI systems have much poorer quality of materials and availability of substrates. Among the many undesirable characteristics of the materials are low thermal conductivity and excessive susceptibility to damage during processing. The IV-VI system identified as most favorable is PbEuSSe/PbSe, in which PbEuSSe quaternaries of different alloy compositions are used for both the active and cladding layers, which are lattice matched to PbSe substrates. However, this system is judged less promising than the GaInAsSb/AlGaAsSb/GaSb system.

A possible II-VI laser system is HgCdTe lattice matched to CdZnTe. However, this system is not likely to have any advantages over the III-V systems. In addition, it has many disadvantages, including the fact that its materials and device technologies are much less developed.

14. SUBJECT TERMS

diode lasers
infrared lasers
Auger recombination
free-carrier absorption
GaInAsSb material

15. NUMBER OF PAGES

72

16. PRICE CODE

17. SECURITY CLASSIFICATION OF REPORT	18. SECURITY CLASSIFICATION OF THIS PAGE	19. SECURITY CLASSIFICATION OF ABSTRACT	20. LIMITATION OF ABSTRACT
Unclassified	Unclassified	Unclassified	